Bioconjugate Chemistry

Article

pubs.acs.org/bc

High-Density Functionalization and Cross-Linking of DNA: "Click" and "Bis-Click" Cycloadditions Performed on Alkynylated Oligonucleotides with Fluorogenic Anthracene Azides

Suresh S. Pujari,[†,‡] Sachin A. Ingale,[†] and Frank Seela*[,†,‡]

[†]Laboratory of Bioorganic Chemistry and Chemical Biology, Center for Nanotechnology, Heisenbergstraße 11, 48149 Münster, Germany

[‡]Laboratorium für Organische und Bioorganische Chemie, Institut für Chemie neuer Materialien, Universität Osnabrück, Barbarastraße 7, 49069 Osnabrück, Germany

Supporting Information

ABSTRACT: High density functionalization of DNA with ethynyl and octadiynyl side chains followed by CuAAC "click labeling" with 9-azidomethylanthracene was performed. Alkynyl DNA was also cross-linked with fluorogenic 9,10-bis-azidomethylanthracene employing the "bis-click" reaction. By this means the fluorescence of the anthracene moiety was imparted to the virtually nonfluorescent DNA. Phosphoramidites of 8-aza-7-deaza-2′-deoxyadenosine with short and long linker arms in a steric nondemanding 7-position were utilized in solid phase oligodeoxynucleotide synthesis. High density alkynylated DNA—without anthracene residues—was found to be of comparable stability with both long and short linker arms. High density anthracene functionalized DNA became less stable with the short linker compared to that with the long linker connectivity. Interstrand cross-linked homodimers constructed from alkynylated oligonucleotides with fluorogenic 9,10-bis-azidomethylanthracene were hybridized with complementary strands to form double helices. They are more stable when the linker was located at a terminus than in a central position. Short linker anthracene adducts were destabilizing compared to long linker adducts. The fluorogenic anthracene residues not only have a significant effect on the duplex stability, but also impart fluorescence to the species. Fluorescence of cross-linked double helices with long linker connectivity was quenched when the cross-link was in a terminal position and was dequenched when the linker was connecting the two double helices at the center of the molecule. The fluorescence of the anthracene cross-linked double helices was strongly increased (dequenched) when the correct base pair was formed, while no change occurred upon mismatch formation.

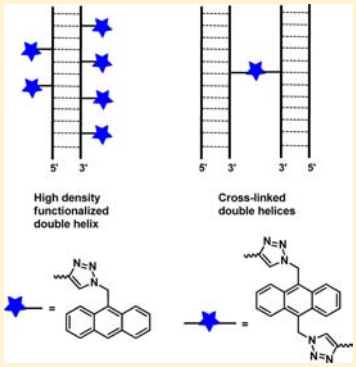

INTRODUCTION

DNA—the storage material of genetic information—has shown great potential for the construction of supramolecular structures.[1−5] Programmable sequence motifs and selective base pairing are ideally suited for the purpose.[6−10] Nature uses their unique recognition system and forms duplexes, triplexes, and multimeric assemblies. Additional functions beyond those in living systems can be added when artificial nucleobases are replacing canonical DNA constituents which then can carry reporter groups or be used as target sites for cross-linking. High density functionalization of DNA[11−13] facilitates the construction of nanoscale devices incorporating specific properties. DNA cross-links are utilized for DNA nanofabrication, as the bottom up strategy requires stable DNA assemblies.[14−17] Reporter groups as well as cross-linkers can be used to integrate additional properties such as fluorescence.[18−20] Multiple labels as well as cross-linkers should be well accommodated in duplex DNA and not disturb the helix structure.[21]

Among various competitive protocols which are used to functionalize DNA, the Cu (I) variant of Huisgen (3 + 2) azide−alkyne cycloaddition (CuAAC) is elegantly suited for the purpose.[22−25] From synthetic biology to material science, this protocol is of paramount importance. Earlier, anthracene mono azide **5** was used for single DNA labeling by the click reaction[26] and nonfluorescent bis-azides were applied to ligate two DNA strands—identical or nonidentical—to construct interstrand cross-links.[27,28] Apart from nucleobase side chain functionalization, the sugar moiety was also utilized[29,30] to subsequently introduce cross-links to stabilize parallel DNA.[31] The click and the stepwise click protocol offer flexibility to cross-link almost every alkynylated DNA which is accessible by automatized oligodeoxynucleotide (ODN) synthesis.

Inspired by the above success, we took one step further where along with the cross-linking of DNA strands, fluorescence was also imparted to DNA by employing a fluorogenic bis-azide in the "bis-click" reaction. Such fluorophore tagging with fluorescent or fluorogenic cross-linkers keeps helical duplex intact and offers a means to visualize and quantify it *in vivo* or *in*

Received: August 1, 2014
Revised: August 22, 2014
Published: August 25, 2014

   dx.doi.org/10.1021/bc5003532 | *Bioconjugate Chem.* 2014, 25, 1855−1870

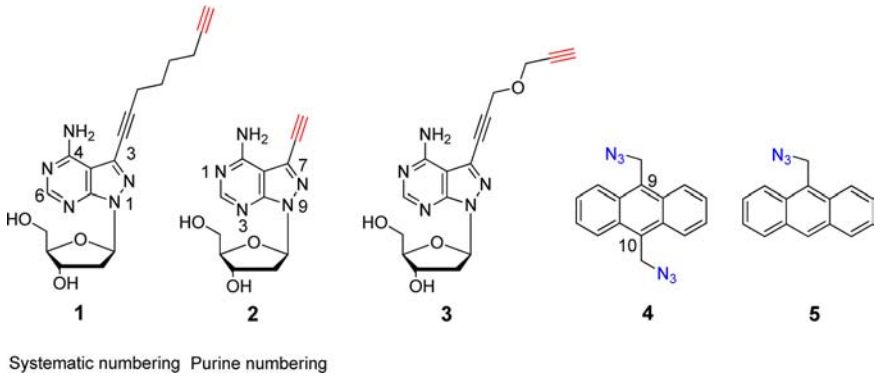

Figure 1. Nucleosides and azides used for the click and "bis-click" functionalization.

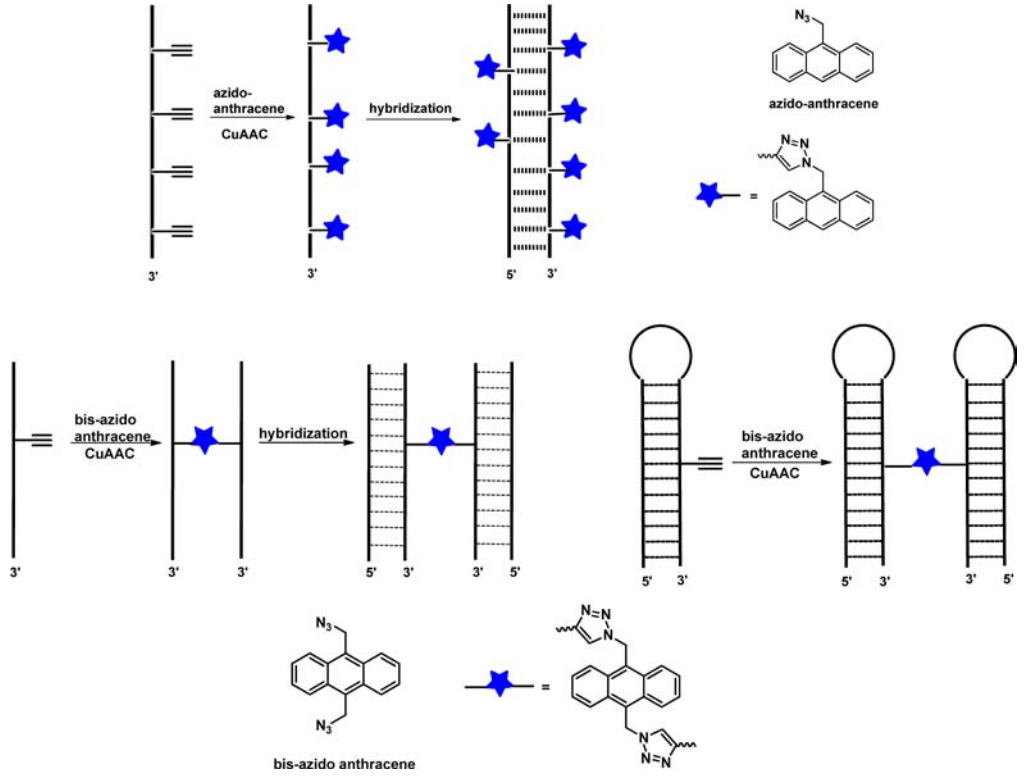

Figure 2. High-density functionalization and interstrand cross-linking of alkynylated DNA with fluorogenic azidomethylanthracenes.

vitro. For fluorescent cross-linking, the fluorogenic bis-azide 9,10-bis-azidomethylanthracene (**4**)[32−34] was selected (Figure 1). Furthermore, high density functionalization of DNA with short and long side chains followed by click functionalization with fluorogenic 9-azidomethyl anthracene **5** was studied.

The nonsubstituted anthracene shows strong violet−blue fluorescence with three absorption bands in the 400 nm region. The advantages of using an anthracene dye as a fluorescent reporter over other fluorogenic residues are its high quantum yield,[34] the distinct absorption pattern,[35] and the ease of preparation.[32−34] Azides **4** and **5** are almost nonfluorescent but are fluorogenic and develop strong fluorescence after click functionalization. Thus, fluorescence can be introduced in the DNA assembly in high density with **5** or by the cross-linker **4**.

For oligodeoxynucleotide functionalization alkynyl derivatives of 8-aza-7-deaza-2′-deoxyadenosine (**1**−**3**) were chosen (Figure 1). They were converted into corresponding phosphoramidites and employed in solid-phase oligonucleotide synthesis. High density functionalization and cross-linking were performed on single strand alkynylated oligonucleotide at various positions. Modified single strands were then hybridized with complementary strands or, in the case of hairpins, cross-linking was performed between the already hybridized stem regions (Figure 2). The influence on duplex stability and fluorescence was compared before and after hybridization as well as their dependence on linker length and positioning.

RESULTS AND DISCUSSION

1. Synthesis and Characterization of Phosphoramidites 9, 12, and Nucleoside Click-Adducts 13, 15−17. The nucleoside **1** and its corresponding phosphoramidite was synthesized as reported.[26] For the synthesis of the new phosphoramidite building blocks **9** and **12**, 8-aza-7-deaza-7-iodo-2′-deoxyadenosine (**6**) was used as a starting material. Sonogashira cross-coupling reaction was performed on **6** with propargyl ether in the presence of CuI, $Pd(PPh_3)_4$, and Et_3N in DMF at room temperature to give the 7-alkynylated nucleoside **3**

dx.doi.org/10.1021/bc5003532 | *Bioconjugate Chem.* 2014, 25, 1855−1870

Scheme 1. Synthesis of Phosphoramidite Building Blocks 9 and 12[a]

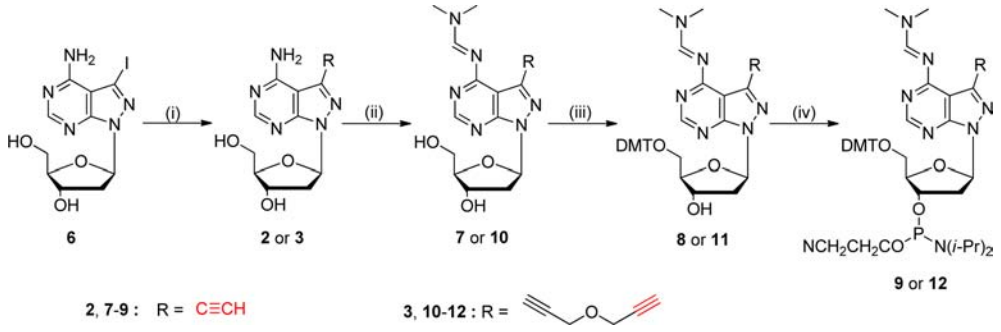

[a]Reagents and conditions: (i) trimethylsilylacetylene or propargyl ether, CuI, $Pd(PPh_3)_4$, Et_3N, DMF, rt, overnight; (ii) *N,N*-dimethylformamide dimethylacetal, MeOH, rt, 1 h; (iii) 4,4′-dimethoxytriphenylmethyl chloride, anhydrous pyridine, rt, 6 h; (iv) 2-cyanoethyl-*N,N* diisopropylchlorophosphoramidite, anhydrous CH_2Cl_2, $(i\text{-Pr})_2EtN$, rt, 30 min.

Scheme 2. Click Functionalization of Nucleosides 1 and 2 with Azide 5

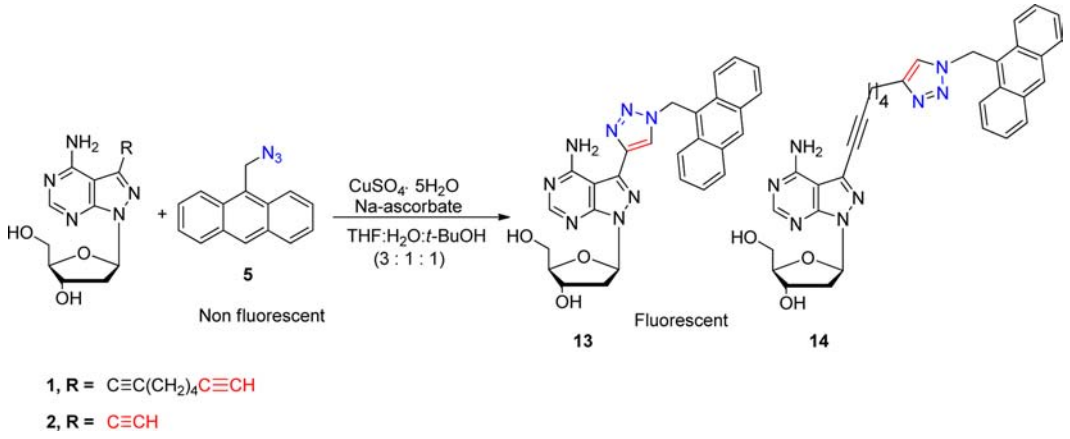

(62%). Nucleoside **2** was synthesized as reported.[36] Protection of the amino groups of **2** and **3** with *N,N*-dimethylformamide dimethylacetal in methanol gave derivatives **7** and **10** in 94% and 86%. Protection of the 5′ hydroxyl groups of **7** and **10** with DMT-Cl and subsequent phosphitylation gave phosphoramidite building blocks **9** and **12** in 65% and 62% yields, respectively (Scheme 1).

Fluorogenic dyes with azido groups can be activated to highly fluorescent molecules by the Cu(I) catalyzed Huisgen-Meldal-Sharpless azide−alkyne cycloaddition (CuAAC), where the azido group becomes part of the triazole system. Those molecules are used to impart the fluorescence to nonfluorescent species via a conjugation process.[26] Having the free alkynylated nucleosides in hand, the concept of fluorogenic click and bis-click functionalization was verified on nucleosides. To this end, 9-azidomethylanthracene (**5**) was used for side chain functionalization and 9,10-bis-azidomethylanthracene (**4**) for bis-click cross-linking. The monofunctionalization with azide **5** was performed on nucleoside **1** (octadiynyl) and **2** (ethynyl); with bis-azide **4**, the cross-linking was studied with the same nucleosides and additionally on nucleoside **3** as well.

The click functionalization of nucleoside **2** with azide **5** was performed in THF:H_2O:*t*-BuOH in the presence of $CuSO_4 \cdot 5H_2O$ as a catalyst and sodium ascorbate as reducing agent. The click reaction proceeds smoothly to give fluorescent click conjugate **13** in 74% yield (Scheme 2). The synthesis and characterization of click conjugate **14** was already reported by our laboratory.[26] It appears that the click functionalization on ethynyl nucleoside **2** proceeds faster compared to nucleoside **1**.

Bis-click cross-linking between respective nucleosides bearing a terminal triple bond (**1**−**3**) and bis-azide **4** was carried out at room temperature in the presence of copper(II) using sodium ascorbate as a reducing agent to give bis-click adducts **15** (70%), **16** (33%), and **17** (48%), respectively (Scheme 3).

All synthesized monomers and cross-linked compounds were characterized by elemental analyses or mass spectra as well as by their ^1H, ^{13}C, and ^{31}P NMR spectra (for spectra see Supporting Information (SI)). DEPT-135 and $^1H-^{13}C$ gated-decoupled NMR spectra were used to assign the ^{13}C NMR signals (SI Table S1).

2. Synthesis and Properties of Oligonucleotides Containing Nucleosides 1 and 2 and Their Click Adducts with 9-Azidomethylanthracene. Earlier studies revealed that 5-alkynyl substituted pyrimidines and 7-alkynyl substituted 7-deazapurines show enhanced duplex stability compared to nonfunctionalized derivatives.[37−40] These side chains are well accommodated in the major groove of DNA rendering greater stability to the duplex.[37−40]

Influence of Alkynyl Residues on Duplex Stability. In this study, the duplex stability of DNA after modification with short and long linkers was compared. Positional as well as high density labeling effects were studied. For this purpose, a series of oligonucleotides containing the building blocks **1**−**3** was synthesized (Table 1) (for MALDI-TOF masses, see SI Table S2). For the hybridization studies, the oligonucleotide duplex 5′-

dx.doi.org/10.1021/bc5003532 | *Bioconjugate Chem.* 2014, 25, 1855−1870

Scheme 3. "Fluorogenic Bis-Click" Reactions of Nucleosides 1−3 with Bis-Azide 4

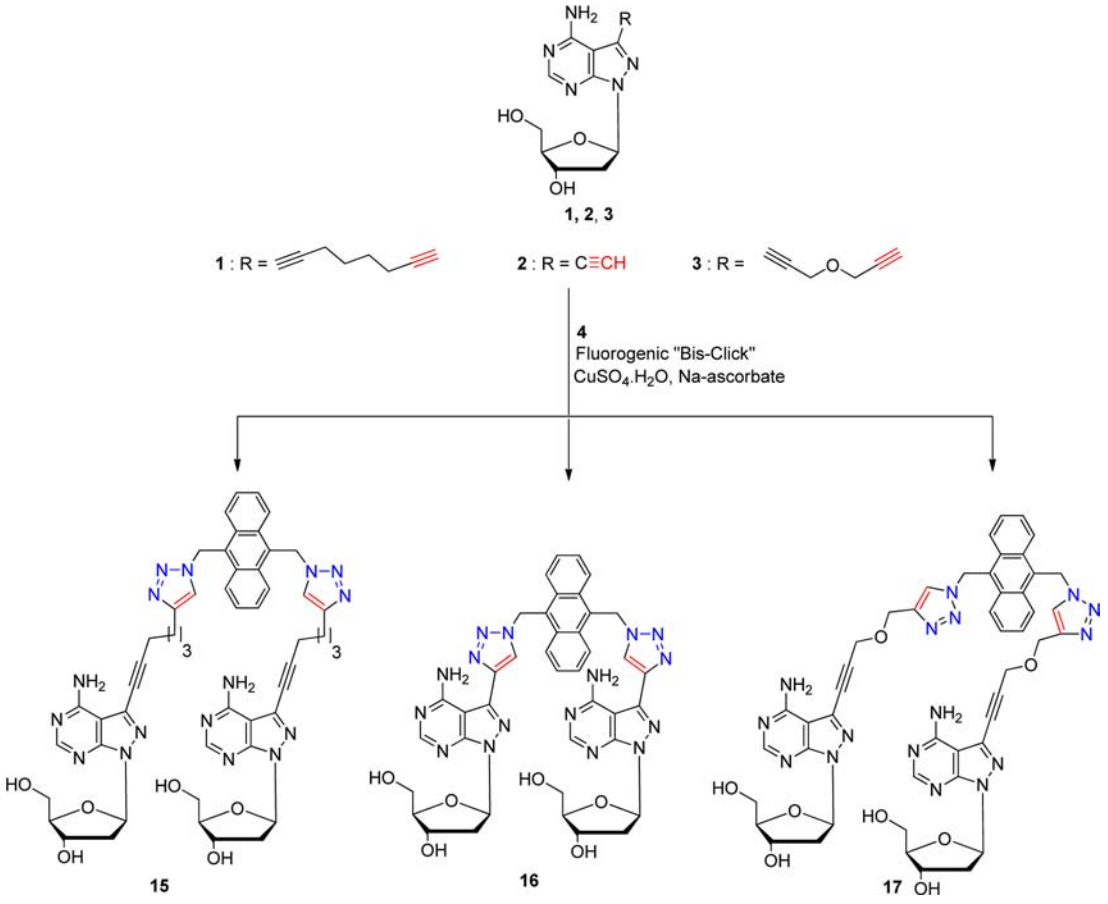

Table 1. T_m-Values of Oligonucleotide Duplexes Containing Alkynylated Nucleosides and Dye Conjugates[a]

Alkynylated Duplexes (Long linker)	T_m[c] [°C]	ΔT_m[b] [°C]	Anthracene Clicked Duplexes (Long linker)	T_m [°C]	ΔT_m[b] [°C]	Alkynylated Duplexes (Short linker)	T_m [°C]	ΔT_m[b] [°C]	Anthracene Clicked Duplexes (Short linker)	T_m [°C]	ΔT_m[b] [°C]
5′-d(TAG GTC AAT ACT) (**18**) 3′-d(ATC CAG TTA TGA) (**19**)	50	--	--	--	--	--	--	--	--	--	--
5′-d(TAG GTC **1**AT ACT) (**20**) 3′-d(ATC CAG TTA TGA) (**19**)	51	+1	5′-d(TAG GTC **14**AT ACT) (**25**) 3′-d(ATC CAG TTA TGA) (**19**)	59[c]	+9	5′-d(TAG GTC **2**AT ACT) (**30**) 3′-d(ATC CAG TTA TGA) (**19**)	52	+2	5′-d(TAG GTC **13**AT ACT) (**35**) 3′-d(ATC CAG TTA TGA) (**19**)	45	-5
5′-d(TAG GTC AAT ACT) (**18**) 3′-d(ATC CAG TTA TG**1**) (**21**)	52	+2	5′-d(TAG GTC AAT ACT) (**18**) 3′-d(ATC CAG TTA TG**14**) (**26**)	55	+5	5′-d(TAG GTC AAT ACT) (**18**) 3′-d(ATC CAG TTA TG**2**) (**31**)	52	+2	5′-d(TAG GTC AAT ACT) (**18**) 3′-d(ATC CAG TTA TG**13**) (**36**)	50	0
5′-d(TAG GTC **1 1**T ACT) (**22**) 3′-d(ATC CAG TTA TGA) (**19**)	54	+4	5′-d(TAG GTC **14 14**T ACT) (**27**) 3′-d(ATC CAG TTA TGA) (**19**)	60	+10	5′-d(TAG GTC **2 2**T ACT) (**32**) 3′-d(ATC CAG TTA TGA) (**19**)	55	+5	5′-d(TAG GTC **13 13**T ACT) (**37**) 3′-d(ATC CAG TTA TGA) (**19**)	40	-10
5′-d(TAG GTC AAT ACT) (**18**) 3′-d(ATC C**1**G TT**1** TGA) (**23**)	53	+3	5′-d(TAG GTC AAT ACT) (**18**) 3′-d(ATC C**14**G TT**14** TGA) (**28**)	62	+12	5′-d(TAG GTC AAT ACT) (**18**) 3′-d(ATC C**2**G TT**2** TGA) (**33**)	55	+6	5′-d(TAG GTC AAT ACT) (**18**) 3′-d(ATC C**13**G TT**13** TGA) (**38**)	35	-15
5′-d(T**1**G GTC **1 1**T **1**CT) (**24**) 3′-d(ATC CAG TTA TGA) (**19**)	56	+6	5′-d(T**14**G GTC **14 14**T **14**CT) (**29**) 3′-d(ATC CAG TTA TGA) (**19**)	62	+12	5′-d(T**2**G GTC **2 2**T **2**CT) (**34**) 3′-d(ATC CAG TTA TGA) (**19**)	55	+5	5′-d(T**13**G GTC **13 13**T **13**CT) (**39**) 3′-d(ATC CAG TTA TGA) (**19**)	-[d]	-
5′-d(TAG GTC **1**AT ACT) (**20**) 3′-d(ATC CAG TTA TG**1**) (**21**)	51	+1	5′-d(TAG GTC **14**AT ACT) (**18**) 3′-d(ATC CAG TTA TG**14**) (**26**)	63	+13	5′-d(TAG GTC **2**AT ACT) (**30**) 3′-d(ATC CAG TTA TG**2**) (**31**)	52	+2	5′-d(TAG GTC **13**AT ACT) (**35**) 3′-d(ATC CAG TTA TG**13**) (**36**)	45	-5
5′-d(TAG GTC **1**AT ACT) (**20**) 3′-d(ATC C**1**G TT**1** TGA) (**23**)	55	+5	5′-d(TAG GTC **14**AT ACT) (**25**) 3′-d(ATC C**14**G TT**14** TGA) (**28**)	68	+18	5′-d(TAG GTC **2**AT ACT) (**30**) 3′-d(ATC C**2**G TT**2** TGA) (**33**)	50	+0	5′-d(TAG GTC **13**AT ACT) (**35**) 3′-d(ATC C**13**G TT**13** TGA) (**38**)	34	-16
5′-d(TAG GTC **1 1**T ACT) (**22**) 3′-d(ATC CAG TTA TG**1**) (**21**)	54	+4	5′-d(TAG GTC **14 14**T ACT) (**27**) 3′-d(ATC CAG TTA TG**14**) (**26**)	64	+14	5′-d(TAG GTC **2 2**T ACT) (**32**) 3′-d(ATC CAG TTA TG**2**) (**31**)	54	+4	5′-d(TAG GTC **1313**T ACT) (**37**) 3′-d(ATC CAG TTA TG**13**) (**36**)	46	-4
5′-d(TAG GTC **1 1**T ACT) (**22**) 3′-d(ATC C**1**G TT**1** TGA) (**23**)	59	+9	5′-d(TAG GTC **14 14**T ACT) (**27**) 3′-d(ATC C**14**G TT**14** TGA) (**28**)	64	+14	5′-d(TAG GTC **22**T ACT) (**32**) 3′-d(ATC C**2**G TT**2** TGA) (**33**)	58	+8	5′-d(TAG GTC **13 13**T ACT) (**37**) 3′-d(ATC C**13**G TT**13** TGA) (**38**)	-[d]	-
5′-d(T**1**G GTC **1 1**T **1**CT) (**24**) 3′-d(ATC CAG TTA TG**1**) (**21**)	57	+7	5′-d(T**14**G GTC **14 14**T **14**CT) (**29**) 3′-d(ATC CAG TTA TG**14**) (**26**)	65	+15	5′-d(T**2**G GTC **2 2**T **2**CT) (**34**) 3′-d(ATC CAG TTA TG**2**) (**31**)	56	+6	5′-d(T**13**G GTC **13 13**T **13**CT) (**39**) 3′-d(ATC CAG TTA TG**13**) (**36**)	-[d]	-
5′-d(T**1**G GTC **1 1**T **1**CT) (**24**) 3′-d(ATC C**1**G TTA TG**1**) (**23**)	60	+10	5′-d(T**14**G GTC **14 14**T **14**CT) (**29**) 3′-d(ATC C**14**G TTA TG**14**) (**28**)	65	+15	5′-d(T**2**G GTC **2 2**T **2**CT) (**34**) 3′-d(ATC C**2**G TTA TG**2**) (**33**)	60	+10	5′-d(T**13**G GTC **13 13**T **13**CT) (**39**) 3′-d(ATC C**13**G TTA TG**13**) (**38**)	-[d]	-

[a]Measured at 260 nm in 1 M NaCl, 100 mM $MgCl_2$, and 60 mM Na-cacodylate (pH 7.0) with 5 μM + 5 μM single-strand concentration. [b]Refers to the temperature difference of the modified duplex versus the unmodified reference duplex. [c]Ref 26. [d]Not dectected.

d(TAG GTC AAT ACT) (**18**) and 3′-d(ATC CAG TTA TGA) (**19**) was chosen as reference duplex, which was further modified at various positions with alkynyl modified nucleosides **1** and **2**. One of the dA residues was replaced by the alkynyl modified

dx.doi.org/10.1021/bc5003532 | *Bioconjugate Chem.* 2014, 25, 1855−1870

Scheme 4. "Click" Reaction of Oligonucleotides Containing 1 and 2 with Azide 5

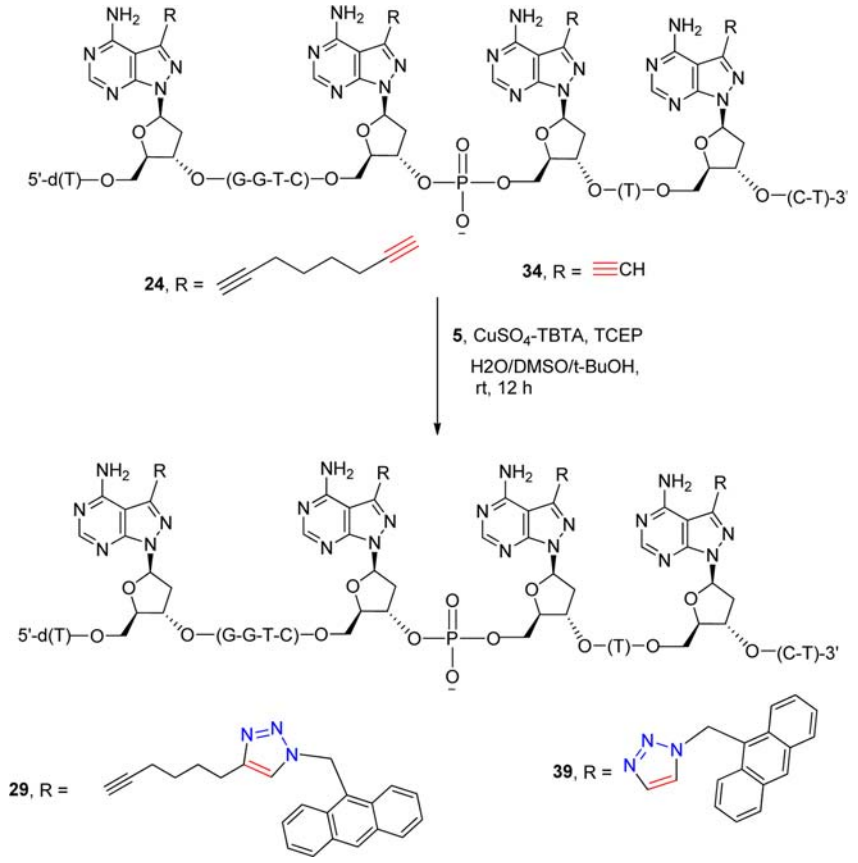

Scheme 5. "Bis-Click" Reaction of Oligonucleotides Containing 1−3 with Bis-azide 4

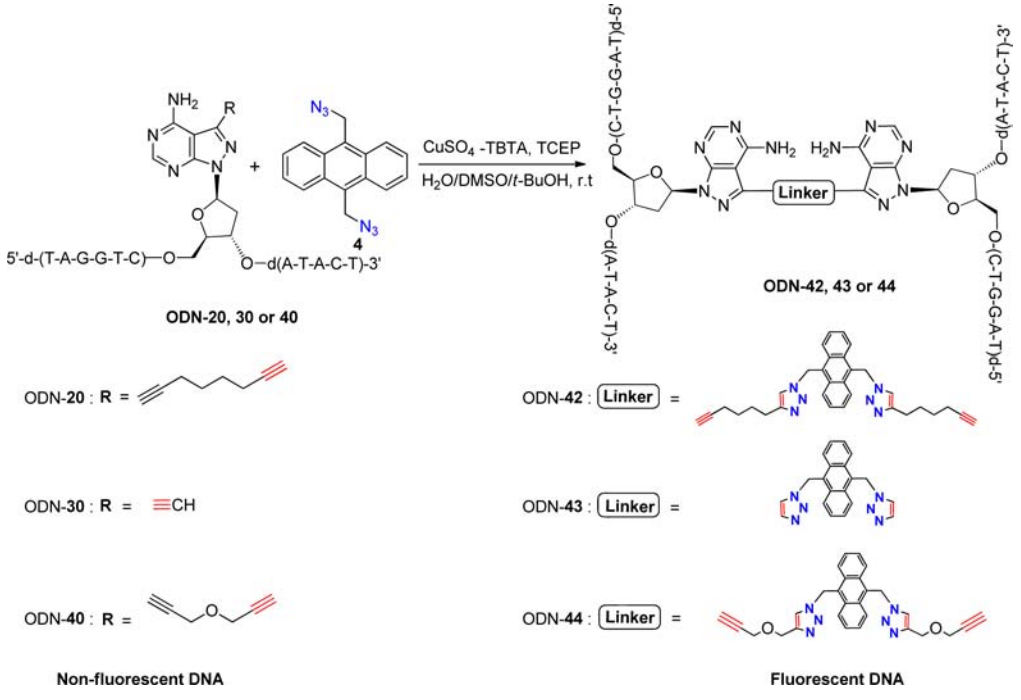

residues **1** and **2** and melting studies were performed. As shown in Table 1, this resulted in about 1 °C (**20**·**19**) and 2 °C (**18**·**21**) increase of T_m value per modification for the octadiynyl linker, whereas a 2 °C increase for the short ethynyl linker (**30**·**19**) and (**18**·**31**) was observed (Table 1). When one strand is modified with two alkynyl residues and hybridized with the unchanged complementary strand, a 5 and 6 °C increase in each duplex containing ethynyl nucleoside **2** (**19**·**32** and **18**·**33**), respectively, against 4 °C (**22**·**19**), and 3 °C (**18**·**23**) increase of 1,7-octadiynyl substituted residues was observed.

dx.doi.org/10.1021/bc5003532 | *Bioconjugate Chem.* 2014, 25, 1855−1870

Scheme 6. Interstrand Cross-Linking of a Hairpin with Fluorogenic Azide 4

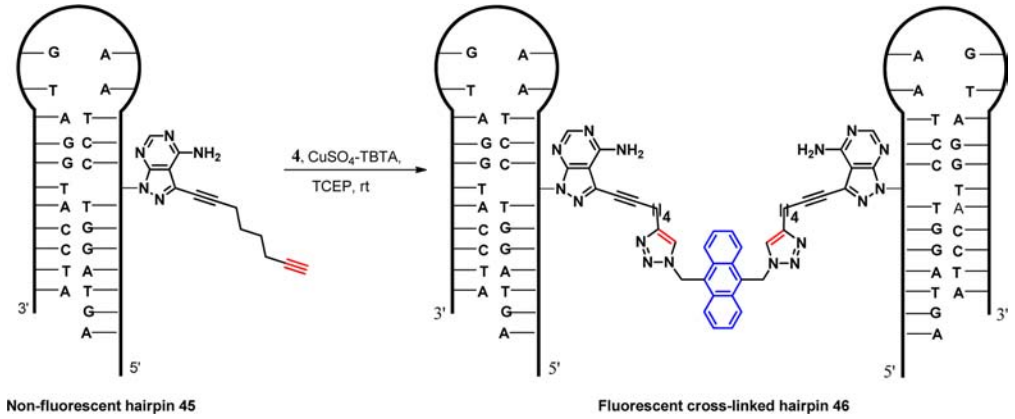

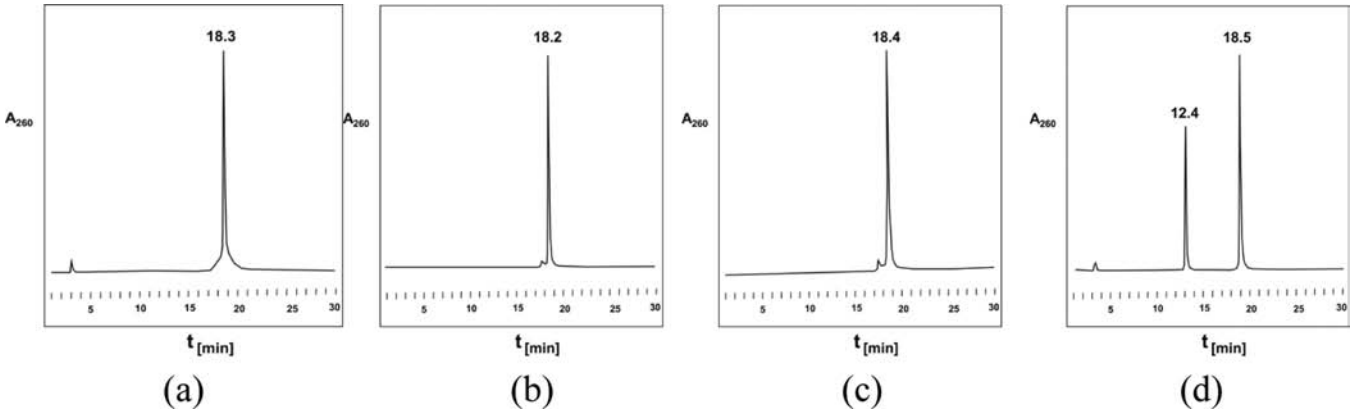

Figure 3. Ion-exchange HPLC elution profiles of (a) cross-linked ODN **43**; (b) cross-linked ODN **44**; (c) cross-linked ODN **52**; (d) artificial mixture of alkynylated ODN **20**; and interstrand cross-linked ODN **42**. Ion-exchange chromatography was performed on a 4 × 250 mm DNA Pac PA-100 column, using the following buffer system: (A) 25 mM Tris-HCl, 10% MeCN, pH 7.0; (B) 25 mM Tris-HCl, 1.0 M NaCl, and 10% MeCN, pH 7.0. Elution gradient: 0−30 min 20−80% B in A with a flow rate of 0.75 mL min^{-1}.

These encouraging results prompted us to perform high density labeling and replace all four dA residues in one strand and hybridize this strand with unchanged complementary strand. T_m measurement results showed a 5 °C increase in the case of ethynyl nucleoside (**34·19**), and a 6 °C increase in the case of octadiynyl nucleoside (**24·19**). The above findings led us to conclude that both the nucleosides—with short and long linker arms—have comparable effects on the stability of modified DNA duplexes.

Influence of Anthracene Click Adducts on the Duplex Stability. Earlier work reports on the effect of one anthracene click conjugate with an octadiynyl linker on the stability of the duplex.[26] Here, we want to investigate the effect of multiple long anthracene click conjugates and compare their effect with ethynyl anthracene click conjugates on duplex stability. For postsynthetic high density functionalization, the click reaction was performed on oligonucleotides containing alkynyl modified residues (Scheme 4, SI Figures S1 and S2). The click reactions were performed in the presence of $CuSO_4$-TBTA [Copper sulfate-Tris(benzyltriazolylmethyl)amine] complex using TCEP (tris-(carboxyethyl)phosphine) as a reducing agent (for details, see Experimental Section, and for masses, see SI Table S2).

When one of the alkynyl dA residues is replaced by anthracene click conjugate **13** (short linker), a decrease in the duplex stability was observed (**35·19** and **18·36**), while an increase in duplex stability was found (**18·26** and **25·19**) when the anthracene click conjugate **14** (long linker) was employed. It is observed from Table 1 that an increased number of anthracene click conjugates with short linkers (**13**) decreases the stability of the duplex. When four or more than four residues of click conjugate **13** were incorporated in oligonucleotides, no duplexes were formed. On the contrary, an increase in the number of anthracene click conjugates having the long linker **14** increases the stability of the duplex.

Based on the above findings the following conclusions can be drawn: (i) Oligonucleotide duplexes bearing both nucleosides with alkynyl side chains (nucleosides **1** and **2**) are of comparable stability (Table 1). (ii) Duplex destabilization was observed in the case of oligonucleotides with high density functionalization by short ethynyl linker click adduct **13**. (iii) A long linker increases the duplex stability of an anthracene high density functionalized duplex.

3. Oligonucleotides with Anthracene Cross-Links. Next, the concept of installing fluorescence along with interstrand cross-link via a fluorogenic bis-click reaction was performed on oligonucleotides. The same oligonucleotide duplex **18·19** was chosen for cross-linking as before for high-density functionalization. This standard duplex was modified at different positions with alkynyl nucleosides **1**−**3** as shown in Scheme 5. Exemplarily, the reaction was carried out on the stem region of hairpin (Scheme 6). The synthesized oligonucleotides were characterized by MALDI-TOF mass spectra (Table S3; for structures, see Figure S3, Supporting Information). The cross-linking was performed on the identical single stranded oligonucleotides **20**,

dx.doi.org/10.1021/bc5003532 | *Bioconjugate Chem.* 2014, 25, 1855−1870

Scheme 7. Fluorogenic Multiple Cross-Linking of DNA by Simultaneous Double "Bis-Click Chemistry"

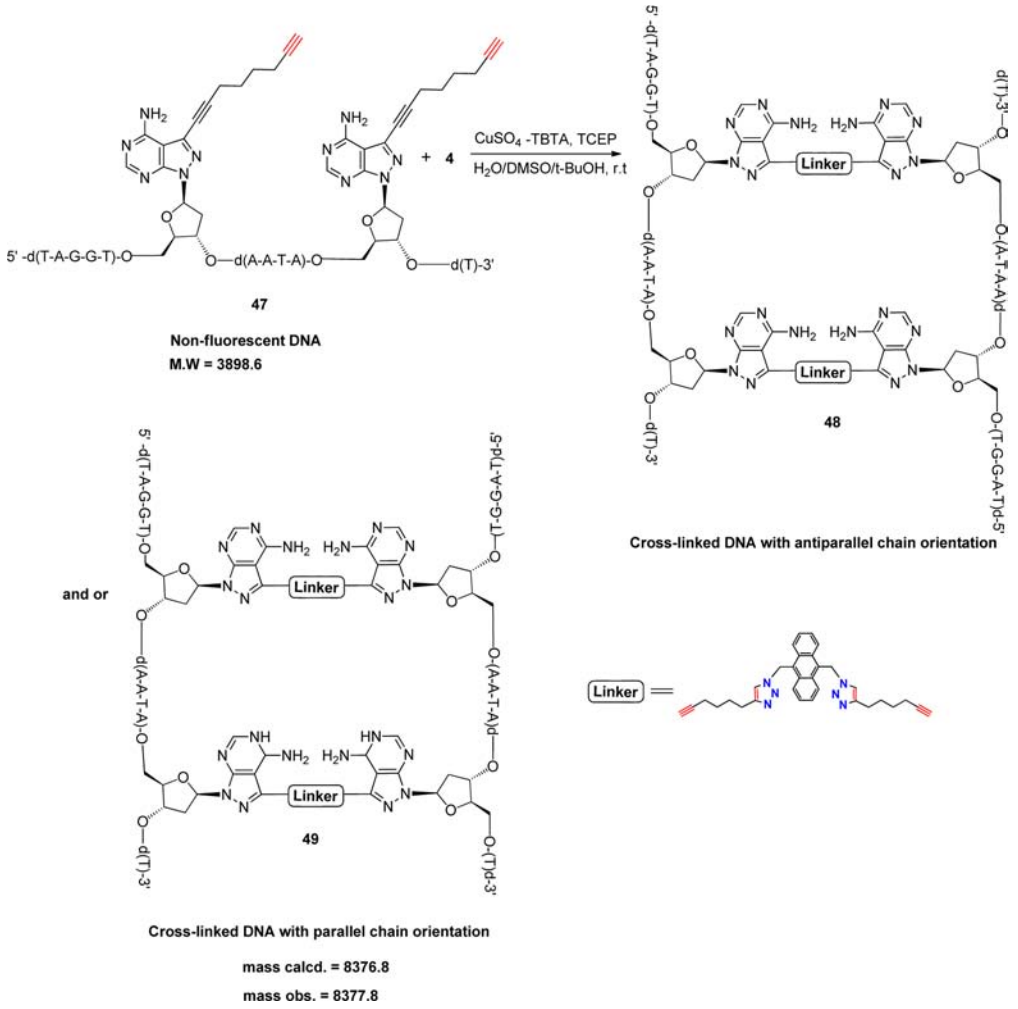

30, and **40** or with hairpin **45** to give interstrand cross-linked (ICL) homodimers (**42**−**44**) or the cross-linked hairpin **46**. The bis-click reaction was performed with anthracene bis-azide **4** in the presence of copper(II) using TCEP as a reducing agent (for details see Experimental Section).

Along with MALDI-TOF characterization, the cross-linked oligonucleotides were analyzed by ion-exchange HPLC. As shown in Figure 3 (Figure S6, Supporting Information), the cross-linked homodimers show a retention times of 18.3−18.5 min, while the retention time of the alkynylated oligonucleotide is 12.4 min. The higher retention time of oligonucleotides **42**, **43**, **44**, and **52** correspond to the increased number of negative phosphate charges which confirms the formation of the cross-link.

Furthermore, the potential of the bis-click cross-link reaction to simultaneously connect the strands at various points was evaluated. As shown in Scheme 7, oligonucleotide **47** containing two residues of alkynylated nucleoside **1** was synthesized. These two modified residues were separated by four base pairs. Then, the bis-click reaction was performed in a DMSO/H_2O mixture with bis-azide **4** to give doubly cross-linked oligonucleotide either **48** or **49** (for structure, see Figure S4, Supporting Information). Assignment of chain orientation was not performed. Next, this oligonucleotide was characterized by MALDI-TOF spectra. The expected value agrees with the observed value confirming the formation of the product. By this means, multiple cross-links can be introduced.

Such cross-linking is valuable since this method can be used to generate end sealed oligonucleotides,[41] when the modification sites are at the end of the chain.[42,43] The cross-link produces oligonucleotides with a cavity like space in between the two strands which might be used as crown ethers in host−guest phenomena and can be used for metal binding as well as catalytic studies.[44]

4. Stability of Cross-Linked Double Helices and Ligated Hairpin. To evaluate the effect of 9,10-bisazidomethylanthracene on cross-linked duplexes or hairpin, the cross-links were introduced at different positions. When the cross-link was installed at the terminal position of the oligonucleotides as in ds **18·50·18**, ds **18·51·18**, and ds **18·52·18**, it caused stabilization of the duplexes by +1 °C to +4 °C. However, when the cross-link was introduced in a central position, slight destabilization of the duplexes was observed (duplexes **19·42·19**, **19·43·19**, and **19·44·19**) (Table 2). However, this effect is more profound when the linker arm is short (ds **19·43·19**). It is concluded that the terminal sites are more flexible to accept the cross-link, while central cross-linking leads to helix distortion. Long flexible linkers are favored over short rigid linkers as linker arms for cross-linking. The cross-linking unit 9,10-bisazidomethylanthracene (**4**) is a favorable linker, since it stabilizes the cross-linked

dx.doi.org/10.1021/bc5003532 | *Bioconjugate Chem.* 2014, 25, 1855−1870

Table 2. T_m Values of Oligonucleotide Duplexes and Cross-Linked Duplexes Containing Alkynyl Side Chains[a,b]

DNA Duplexes	T_m [°C]	Cross-linked duplexes	T_m [°C]
3'-d(ATC CAG TTA TGA)-5'(**19**) 5'-d(TAG GTC **1**AT ACT)-3' | (**42**) 5'-d(TAG GTC **1**AT ACT)-3' 3'-d(ATC CAG TTA TGA)-5' (**19**)	51	5'-d(TAG GTC AAT ACT)-3' (**18**) 3'-d(ATC CAG TTA TG**1**)-5' | (**50**) 3'-d(ATC CAG TTA TG**1**)-5' 5'-d(TAG GTC AAT ACT)-3' (**18**)	55
3'-d(ATC CAG TTA TGA)-5'(**19**) 5'-d(TAG GTC **2**AT ACT)-3' | (**43**) 5'-d(TAG GTC **2**AT ACT)-3' 3'-d(ATC CAG TTA TGA)-5' (**19**)	43	5'-d(TAG GTC AAT ACT)-3' (**18**) 3'-d(ATC CAG TTA TG**2**)-5' | (**51**) 3'-d(ATC CAG TTA TG**2**)-5' 5'-d(TAG GTC AAT ACT)-3' (**18**)	51
5'-d(TAG GTC **3**AT ACT) (**40**) 3'-d(ATC CAG TTA TGA) (**19**)	52	3'-d(ATC CAG TTA TGA)-5'(**19**) 5'-d(TAG GTC **3**AT ACT)-3' | (**44**) 5'-d(TAG GTC **3**AT ACT)-3' 3'-d(ATC CAG TTA TGA)-5' (**19**)	47
5'-d(TAG GTC AAT ACT) (**18**) 3'-d(ATC CAG TTA TG**3**) (**41**)	52	5'-d(TAG GTC AAT ACT)-3' (**18**) 3'-d(ATC CAG TTA TG**3**)-5' | (**52**) 3'-d(ATC CAG TTA TG**3**)-5' 5'-d(TAG GTC AAT ACT)-3' (**18**)	52

Hairpins	T_m [°C]
5'-d(AGT AGG TAC CTA AGT AGG TAC CTA)-3' (**53**)	75
5'-d(AGT AGG T**I**C CTA AGT AGG TAC CTA)-3' (**45**)	76
5'-d(AGT AGG T**I**C CTA AGT AGG TAC CTA)-3' | (**46**) 5'-d(AGT AGG T**I**C CTA AGT AGG TAC CTA)-3'	76

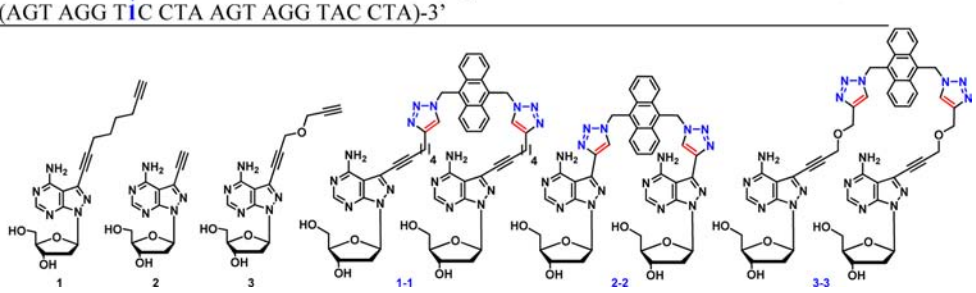

[a]Measured at 260 nm in 1 M NaCl, 100 mM $MgCl_2$, and 60 mM Na-cacodylate (pH 7.0) with 5 μM single-strand concentration of each strand in non-cross-linked duplexes and 5 μM of cross-linked duplexes. [b]T_m values were determined from the melting curves by using the program MeltWin 3.0.

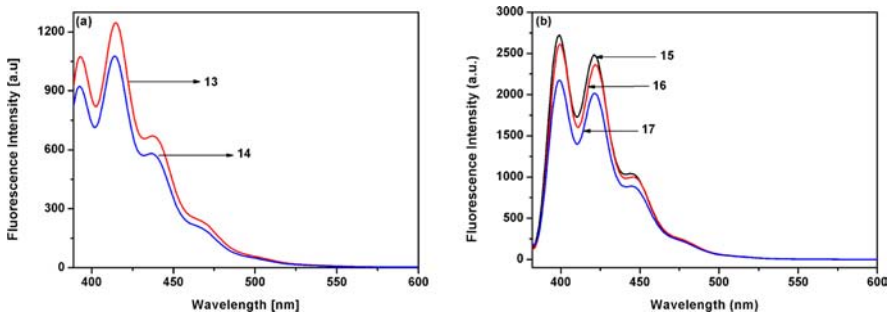

Figure 4. Emission spectra of (a) anthracene nucleoside click adducts **13**, **14** (excitation wavelength 365 nm); (b) anthracene cross-linked click adducts **15**–**17** (excitation wavelength 371 nm). The samples were dissolved in 99.5 mL methanol and 0.5 mL DMSO and spectra were recorded. For the details, see Experimental Section.

oligonucleotides. The stability of the hairpin is not affected by cross-linking (Table 2).

5. Anthracene Fluorescence of Functionalized and Cross-Linked Nucleosides and Oligonucleotides. *Nucleoside Anthracene Click and Bis-Click Adducts.* Anthracene azides were chosen owing to the favorable properties of the anthracene unit.[35,45−50] All fluorescence measurements on nucleosides were performed in methanol (containing 0.5%

dx.doi.org/10.1021/bc5003532 | Bioconjugate Chem. 2014, 25, 1855−1870

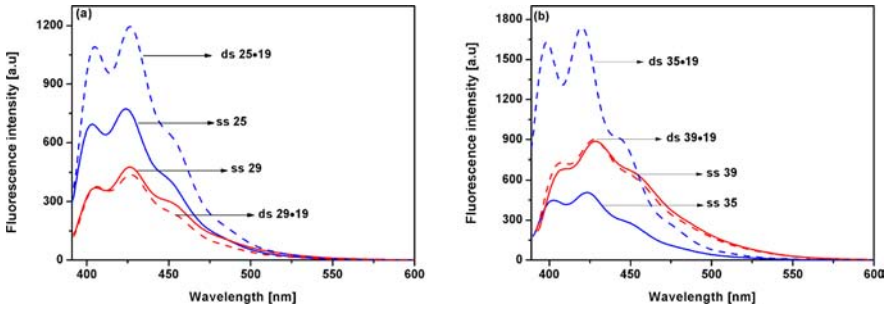

Figure 5. Fluorescence emission spectra of (a) single stranded and duplex oligonucleotides containing anthracene long linkers. (b) Single stranded and duplex oligonucleotides containing anthracene short linkers. Measurements were performed in 1 M NaCl, 100 mM $MgCl_2$, and 60 mM Na-cacodylate (pH 7.0). For the details, see Experimental Section.

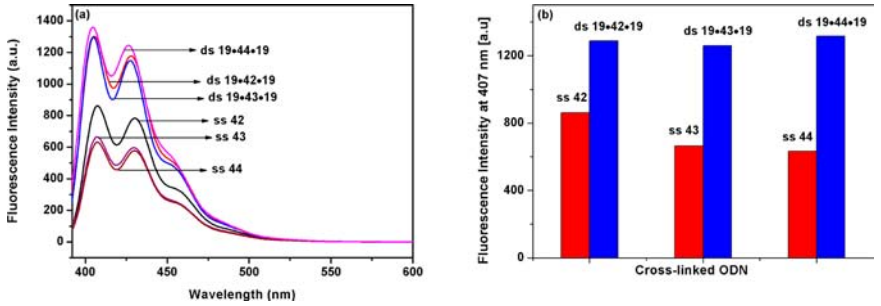

Figure 6. Fluorescence intensity of (a) single stranded cross-linked oligonucleotides and their corresponding duplexes. (b) Bar diagram of the corresponding fluorescence intensities. In all these cross-linked ODNs the cross-link is located at the center of the oligonucleotide. Measurements were performed in 1 M NaCl, 100 mM $MgCl_2$, and 60 mM Na-cacodylate (pH 7.0). For the details, see Experimental Section.

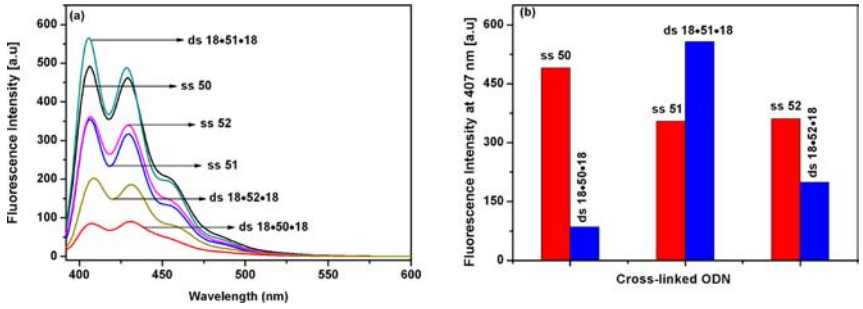

Figure 7. Fluorescence intensity of (a) single stranded cross-linked oligonucleotides and their corresponding duplexes. (b) Bar diagram of the corresponding fluorescence intensities. In all these cross-linked ODNs the cross-link is located at the terminus of the oligonucleotide. Measurements were performed in 1 M NaCl, 100 mM $MgCl_2$, and 60 mM Na-cacodylate (pH 7.0). For the details, see Experimental Section.

DMSO). The absorption and emission spectra of both compounds **13** and **14** and bis-click cross-link adducts **15**−**17** show three distinctive bands corresponding to anthracene unit and look relatively similar (Figure 4) (Figure S7, SI). As shown in Figure 4b, click conjugates **15** and **16** display higher fluorescence intensity compared to the click conjugate **17** containing a propargyl ether linker. The decrease in the fluorescence intensity might be attributed to the differences in polarity or the electronic nature of the various linkers.

Anthracene Fluorescence of High-Density Functionalized Oligonucleotides. The thermal studies reveal that, upon high-density click functionalization of a short linker chain with bulky reporter group, duplex formation is highly restricted. However, on contrary, in all cases the duplexes are formed when long linker click adducts were employed. To evaluate the influence of different linker lengths, fluorescence measurements of the oligonucleotide anthracene click adducts were performed as single strands and in duplexes. These studies led us to make the following conclusions: (i) The ss-ODN **25** containing one long linker anthracene click conjugate (**14**) shows higher fluorescence intensity compared to ss-ODN **29** containing four anthracene click conjugates (Figure 5a). (ii) The fluorescence intensity of ODN **25** increases upon duplex formation (duplex **25·19**) whereas fluorescence remains almost unchanged for duplex **29·19** (Figure 5a). (iii) In short linker anthracene oligonucleotide click conjugates, fluorescence intensity increases as the number of anthracene click conjugates (**13**) increased in single stranded oligonucleotides from one modified ss-ODN **35** to four modified ss-ODN **39** (Figure 5b). However, the fluorescence increase does not amount to the number of added anthracene residues. This might be the result of self-quenching or anthracene intercalation.[51,52] (iv) Fluorescence intensity of ODN **35** increases upon duplex formation (duplex **35·19**), whereas fluorescence remains almost unchanged for ODN **39** (duplex **39·19**) (Figure 5b).

dx.doi.org/10.1021/bc5003532 | *Bioconjugate Chem.* 2014, 25, 1855−1870

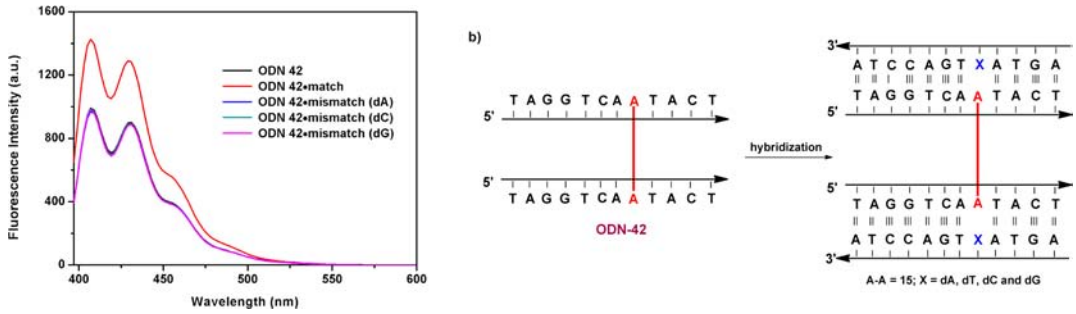

Figure 8. (a) Fluorescence spectra of single base mismatch discrimination of central cross-linked oligonucleotide **42**. (b) Schematic presentation of the mismatch situation. Measurements were performed in 1 M NaCl, 100 mM $MgCl_2$, and 60 mM Na-cacodylate (pH 7.0). For the details, see Experimental Section.

According to the T_m data (Table 1), the highly modified single strand **39** with the short linker connectivity did not form a duplex. According to that no fluorescence change is observed in the presence of the complementary strand.

In summary, it is evident that the rigid short linkers are the best choice for high-density functionalization to obtain highly fluorescent oligonucleotides compared to the oligonucleotides containing the long flexible linkers. Long linkers give the anthracene moieties enough flexibility to interact with each other. This causes substantial fluorescence quenching and might lead to fluorescence properties in which the intensity is higher for single dye modification than for high-density functionalized molecules. But the short linker does have an adverse effect upon high-density click functionalization on the stability of the duplex whereas no such phenomenon was observed in the case of click conjugates with the long linker arm. However, in all cases, the microenvironment around each anthracene unit, $\pi-\pi$ stacking, FRET, and electron tunneling factors must be taken into consideration.

Fluorescence of Oligonucleotides with Anthracene Cross-Links. Then, the influence of the cross-linking point on the fluorescence intensity and its behavior in DNA has been studied. After cross-linking, the oligonucleotide homodimers were hybridized with complementary strands and the fluorescence intensity changes were studied. When the fluorescence intensity of homodimers with terminal cross-linking positions was compared to those with central positions, the oligonucleotide with cross-links at the center of the duplex show higher fluorescence intensity than the ODN with terminal cross-links (Figures 6 and 7). Upon duplex formation, the fluorescence of oligonucleotides always increases as shown in Figure 6, when the cross-link is at the center of the duplex. It is anticipated that the more rigid nature of the duplex is attributed to the dequenching phenomenon.

Upon hybridization of terminally cross-linked homodimers to double helices, the fluorescence intensity quenches significantly. Surprisingly, the fluorescence intensity increases upon duplex formation when the cross-link was at the end of the duplex with the short rigid linker (ethynyl) (Figure 7).

Exemplarily, the thermal stability and fluorescence intensity of the cross-linked hairpin was studied (see Figure S8, Supporting Information). The cross-link does not have an adverse effect on the stability of the hairpin (Table 2).

Single Base Mismatch Discrimination of Anthracene Cross-Linked Oligonucleotides. Mismatch discrimination studies were performed with one cross-linked oligonucleotide. In this setup, the fluorescent anthracene cross-link unit was used as sensor unit.[53,54] To this end oligonucleotide **42** was chosen with the anthracene cross-link at the center of the homodimer. Then, the fluorescence changes were measured against the mismatch bases dA, dG, and dC and fully matched duplex (dT). As shown in Figure 8, the fluorescence intensity remains at the single strand level in all the mismatched situations and increases in the homomeric duplex with the correct base pair. Apparently, the micro environment of all three mismatches is similar for the anthracene cross-link. All mismatches provide the anthracene moiety flexibility. However, when the intact base pair is formed, the two double helices stiffen giving the anthracene molecule less freedom to interact with other parts of the molecule, which finally results in an increased fluorescence leading to a positive signal response (dequenching). Although this new detection system does not respond on a particular mismatch it responds in a positive way when the correct base pair is formed.

■ CONCLUSION AND OUTLOOK

High-density "click" functionalization of DNA with a fluorescent anthracene residue was studied and double helices and a hairpin were constructed with fluorescent anthracene cross-links. To this end, new phosphoramidites of 8-aza-7-deaza-2′-deoxyadenosine (**9** and **12**) were synthesized with side chains in sterically nondemanding positions and were employed in solid-phase oligonucleotide synthesis. The influence of the linker length on the high-density anthracene functionalization of oligonucleotides was examined. Short linkers are better suited for the purpose of getting strongly fluorescent oligonucleotides upon high density functionalization, whereas to obtain more stable oligonucleotides with high density of fluorophores, a long linker is advantageous.

"Bis-click" reactions were performed on alkynylated DNA with fluorogenic 9,10 bis-azidomethylanthracene to install cross-links. By this means the fluorescence of the anthracene moiety was integrated to the virtually nonfluorescent DNA. After cross-linking, the homodimers with cross-link were hybridized with complementary strands to yield cross-linked double helices. The ligated molecules show similar stability to non-cross-linked duplexes. Regarding anthracene fluorescence, the intensity depends on the cross-linking position. The fluorescence was quenched upon hybridization when the linker was in a terminal position, while it increases when the linker was connecting the double helices at the center of the molecule. Fluorescence of the cross-linked molecule was also sensitive against single base mismatches when hybridized with complementary strands with the four canonical bases in pairing positions. Fluorescence was strongly increased when the correct base pair was formed. Cross-linked homodimeric DNA can be used as adaptors in DNA origami and for the construction of larger DNA assemblies.

dx.doi.org/10.1021/bc5003532 | *Bioconjugate Chem.* 2014, 25, 1855−1870

Table 3. ^{13}C NMR Chemical Shifts of Nucleosides, Click, and "Bis-Click" Derivatives[a]

	C(2)[b] C(6)[c]	C(4)[b] C(7a)[c]	C(5)[b] C(3a)[c]	C(6)[b] C(4)[c]	C(7)[b] C(3)[c]	C≡C	CH_2	triazole	C(1′)	C(2′)	C(3′)	C(4′)	C(5′)
2[e]	157.6	153.6	101.1	156.8	126.0	86.5 75.0	--	--	84.1	37.9	70.9	87.8	62.3
7	157.7	154.4	108.1	162.2	127.9	84.2 76.3	--	--	84.2	37.9	71.0	87.8	62.4
8	157.6	154.4	108.1	162.1	126.4	85.1 76.4	--	--	84.0	37.9	70.3	85.3	63.9
3	157.6	153.7	100.9	156.7	126.1	90.8 79.6 78.0 77.4	57.2 56.7	--	84.1	37.9	70.9	87.8	62.3
10	157.7	154.5	108.0	162.2	127.7	88.5 79.4 79.0 78.0	56.6 56.4	-	84.1	37.9	71.0	87.7	62.3
11	157.6	154.4	108.0	162.1	126.4	88.2 79.3 79.2 77.9	56.6 56.3	--	83.9	38.0	70.5	85.4	64.1
13	156.5	154.6	100.8	158.2	127.2	96.6 72.1	46.1	140.6 124.0[d]	84.2	37.8	70.9	87.7	62.4
15	157.8	153.6	100.8	156.7	127.3[d]	96.6 72.1	45.5 30.7 27.2 24.4 18.6	146.6 121.7[d]	84.0	37.9	71.0	87.7	62.4
16	156.5	154.6	97.9	158.1	127.0[d]	--	46.3	140.6 124.0[d]	84.2	37.9	71.0	87.7	62.4
17	157.6	153.7	100.9	156.7	126.9[d]	91.3 77.2	45.6 57.6	143.2 124.1[d]	84.1	37.9	70.9	87.8	62.3

[a]Measured in DMSO-d_6 at 298 K. [b]Purine numbering. [c]Systematic numbering. [d]Tentative. [e]ref 36.

EXPERIMENTAL SECTION

General Methods and Materials. All chemicals and solvents were of laboratory grade as obtained from commercial suppliers and were used without further purification. Thin-layer chromatography (TLC) was performed on TLC aluminum sheets covered with silica gel 60 F254 (0.2 mm). Flash column chromatography (FC): silica gel 60 (40−60 μM, for flash chromatography) at 0.4 bar. UV spectra: λ_{max} (ε) in nm, ε in dm^3 mol^{-1} cm^{-1}. NMR spectra were measured at 300.15 MHz for ^{1}H, 75.48 MHz for ^{13}C, and 121.52 MHz for ^{31}P. The J values are given in Hz; δ values are given in ppm relative to Me_4Si as internal standard. For NMR spectra recorded in DMSO-d_6, the chemical shift of the solvent peak was set to 2.50 ppm for ^{1}H NMR and 39.50 ppm for ^{13}C NMR. The ^{13}C NMR signals were assigned on the basis of DEPT-135 and ^{1}H−^{13}C gated-decoupled NMR spectra (Table 3; for coupling constants see Table S1 in the Supporting Information). Reversed-phase HPLC was carried out on a 4 × 250 mm RP-18 (10 μM) LiChrospher 100 column with a HPLC pump connected with a variable wavelength monitor, a controller, and an integrator. ESI-TOF mass spectra of nucleosides were recorded on a Micro-TOF spectrometer. Elemental analyses were performed by Mikroanalytisches Laboratorium Beller (Göttingen, Germany). The ^{13}C NMR chemical shifts are listed in Table 3. Molecular masses of oligonucleotides were determined by MALDI-TOF mass spectrometry in the linear positive mode with 3-hydroxypicolinic acid (3-HPA) as a matrix (Tables S2 and S3, Supporting Information). T_m values were determined from the melting curves using the software MELTWIN, version 3.0 (J. A. McDowell, 1996).

Synthesis, Purification, and Characterization of Oligonucleotides. The oligonucleotides were synthesized on an automated DNA synthesizer on a 1 μmol scale employing standard phosphoramidites as well as the phosphoramidites **9** and **12**. After cleavage from the solid support, the oligonucleotides were deprotected in concentrated aqueous ammonia solution for 16 h at 55 °C. The purification of the "trityl-on" oligonucleotides was carried out on reversed-phase HPLC using the following gradient system at 260 nm: (A) MeCN; (B) 0.1 M (Et_3NH)OAc (pH 7.0):MeCN, 95:5; gradient I: 0−3 min 10−15% A in B, 3−15 min 15−50% A in B, flow rate 0.8 mL/min. The purified "trityl-on" oligonucleotides were treated with 2.5% $CHCl_2COOH/CH_2Cl_2$ for 2 min at 0 °C to remove the 4,4′-dimethoxytrityl residues. The detritylated oligomers were purified again by reversed-phase HPLC with gradient II: 0−20 min, 0−20% A in B, 20−25 min, 20% A in B, flow rate 0.8 mL/min. The oligonucleotides were desalted on a short column (RP-18) using water for elution of salt, while the oligonucleotides were eluted with H_2O:MeOH (2:3). The oligonucleotides were lyophilized on a Speed-Vac evaporator to yield colorless or yellow solids which were frozen at −24 °C. The extinction coefficients of ε_{260} (H_2O) of the nucleosides are dA 15400, dG 11700, dT 8800, dC 7300, **13** 33 200 (MeOH), **15** 107 000 (MeOH), **16** 101 400 (MeOH), and **17** 92 000 (MeOH).

Fluorescence Measurements. *(a). Nucleoside Click Conjugates.* All fluorescence measurements of nucleoside click conjugates **13**−**14** and cross-linked click conjugates **15**−**17** were

dx.doi.org/10.1021/bc5003532 | Bioconjugate Chem. 2014, 25, 1855−1870

performed in MeOH (0.5% DMSO). The UV absorbance of nucleoside click conjugates **13** and **14** were adjusted to identical UV absorbance at 365 nm and excited at this wavelength (Figure 4a). The absorption of bis-click adducts **15**−**17** were also adjusted to identical UV absorbance at 371 nm and excited at this wavelength (Figure 4b).

(b). Oligonucleotide Click Conjugates. The single stranded high-density labeled oligonucleotides (**25**, **29** and **35**, **39**) were taken (2 μM) in 1 mL of 1 M NaCl, 100 mM $MgCl_2$, and 60 mM Na-cacodylate (pH 7.0) buffer and excited at 371 nm, and fluorescence measurements were performed. Then, equal concentration, i.e., 2 μM of complementary strand was added to increase the single strand concentration to 4 μM, and the hybridization was performed and then fluorescence was measured (Figure 5). Similar fluorescence measurement studies were performed on cross-linked oligonucleotides (**42**−**44**, **51**−**52**). The excitation wavelength for cross-linked oligonucleotides is 376 nm (Figures 6 and 7).

1-[2-Deoxy-β-D-*erythro*-pentofuranosyl]-3-ethynyl-4-[(dimethylamino)methylidene] amino-1*H*-pyrazolo[3,4-*d*]pyrimidine (7). To a solution of compound **2**[36] (0.3 g, 1.09 mmol) in MeOH (30 mL) was added *N,N*-dimethylformamide dimethylacetal (3.24 g, 27.2 mmol) and the reaction mixture was stirred at room temperature for 1 h. After completion of the reaction (monitored by TLC), the solvent was evaporated and the residue was subjected to FC (silica gel, column 10 × 4 cm, eluted with CH_2Cl_2/MeOH 97:3 → 90:10). Evaporation of the main zone afforded compound 7 (0.34 g, 94%) as a colorless foam. TLC (CH_2Cl_2/MeOH 9:1). R_f 0.5. λ_{max}(MeOH)/nm 324 (ε/dm^3 mol^{-1} cm^{-1} 27900). ^{1}H NMR [DMSO-d_6, 300 MHz]: δ 2.23−2.31 (m, 1H, C2′-H$_\alpha$), 2.76−2.85 (m, 1H, C2′-H$_\beta$), 3.19 (s, 3H, CH_3), 3.23 (s, 3H, CH_3), 3.49−3.54 (m, 2H, C5′-H), 3.80−3.85 (m, 1H, C4′-H), 4.42−4.45 (m, 1H, C3′-H), 4.48 (s, 1H, C≡CH), 4.80 (t, J = 5.7 Hz, 1H, C5′-OH), 5.32 (d, J = 4.2 Hz, 1H, C3′-OH), 6.58 (t, J = 6.6 Hz, 1H, C1′-H), 8.45 (s, 1H, C2-H), 8.92 (s, 1H, NCH). Anal. Calcd for $C_{15}H_{18}N_6O_3$: C 54.54, H 5.49, N 25.44. Found: C 54.45, H 5.59, N 25.28.

1-(2-Deoxy-5-*O*-(4,4′-dimethoxytrityl)-β-D-*erythro*-pentofuranosyl)-3-(ethynyl)-4-[(dimethylamino)-methylidene]amino]-1*H*-pyrazolo[3,4-*d*]pyrimidine (8). Compound 7 (0.52 g, 1.56 mmol) was dried by repeated coevaporation with dry pyridine (3 × 5 mL). The residue was dissolved in dry pyridine (18 mL) and stirred with 4,4′-dimethoxytrityl chloride (0.63 g, 1.87 mmol) at rt for 6 h. After completion of the reaction (monitored by TLC), methanol (6 mL) was added to the reaction mixture and stirring was continued for another half an hour. Then the reaction mixture was evaporated to dryness under reduced pressure and the remaining residue was dissolved in dichloromethane (50 mL) and extracted with 5% aq $NaHCO_3$ solution (50 mL × 2) and then washed with water (80 mL). The organic layer was dried over anhydrous Na_2SO_4, and the solvent was evaporated under reduced pressure and the residue was subjected to FC (silica gel, column 10 × 4 cm, eluted with CH_2Cl_2/acetone 90:10 → 80:20). Evaporation of the main zone afforded **8** (0.72 g, 73%) as a colorless foam. TLC (silica gel, CH_2Cl_2/MeOH 9:1). R_f 0.6. λ_{max}(MeOH)/nm 323 (ε/dm^3 mol^{-1} cm^{-1} 26 900). ^{1}H NMR [DMSO-d_6, 300 MHz]: δ 2.27−2.36 (m, 1H, C2′-H$_\alpha$), 2.78−2.87 (m, 1H, C2′-H$_\beta$), 2.93−2.99 (m, 1H, C5′-H), 3.04−3.09 (m, 1H, C5′-H), 3.17 (s, 3H, CH_3), 3.22 (s, 3H, CH_3), 3.68 (s, 3H, CH_3), 3.69 (s, 3H, CH_3), 3.90−3.93 (m, 1H, C4′-H), 4.48 (s, 1H, C≡CH), 4.54−4.57 (m, 1H, C3′-H), 5.33 (d, J = 5.1 Hz, 1H, C3′-OH), 6.59−6.63 (m, 1H, C1′-H), 6.70−6.77 (m, 4H, Ar-H), 7.13−7.20 (m, 7H, Ar-H), 7.27−7.29 (m, 2H, Ar-H), 8.48 (s, 1H, C2-H), 8.91 (s, 1H, NCH). Anal. Calcd for $C_{36}H_{36}N_6O_5$: C 68.34, H 5.74, N 13.28. Found: C 68.41, H 5.86, N 13.06.

1-[2-Deoxy-5-*O*-(4,4′-dimethoxytrityl)-β-D-*erythro*-pentofuranosyl)]-3-ethynyl-4-[(dimethylamino)-methylidene]amino-1*H*-pyrazolo[3,4-*d*]pyrimidin-3′-(2-cyanoethyl)-*N,N*-diisopropylphosphoramidite (9). A solution of **8** (0.21 g, 0.33 mmol) in dry CH_2Cl_2 (20 mL) was stirred with (i-Pr)$_2$NEt (148 μL, 0.16 g, 0.67 mmol) at rt. Then, 2-cyanoethyl diisopropylphosphoramidochloridite (113 μL, 0.087 g, 0.67 mmol) was added and the reaction mixture was stirred for 30 min. After completion of the reaction (monitored by TLC), the reaction mixture was diluted with CH_2Cl_2 (30 mL) and was poured into 5% $NaHCO_3$ solution (30 mL) and extracted with CH_2Cl_2 (3 × 30 mL). The combined organic phases were dried over Na_2SO_4 and the solvent was evaporated. The residual foam was applied to FC (silica gel, column 8 × 3 cm, eluted with CH_2Cl_2/acetone 100:0 → 95:5). Evaporation of the main zone afforded **9** (0.18 g, 65%) as a colorless foam. TLC (silica gel, CH_2Cl_2/acetone 9:1). R_f 0.7. ^{31}P NMR ($CDCl_3$, 121 MHz): 148.44, 148.35. ESI-TOF m/z calcd. for $C_{45}H_{52}N_8O_6P$ [M + H$^+$] 833.3898, found 838.3883.

1-[2-Deoxy-β-D-*erythro*-pentofuranosyl]-[3-(prop-2-ynyloxy)prop-1-ynyl]-1*H*-pyrazolo[3,4-*d*]-pyrimidine (3). To a solution of compound **6** (1 g, 2.66 mmol) in dry DMF (15 mL) was added CuI (0.101 g, 0.53 mmol), Pd(PPh$_3$)$_4$ (0.306 g, 0.26 mmol), dry Et_3N (0.538 g, 0.74 mL, 5.32 mmol), and propargyl ether (2.5 g, 2.74 mL, 26.0 mmol). The reaction mixture which slowly turns to black was stirred under inert atmosphere for 12 h (TLC monitoring). The reaction mixture was evaporated and the residue was adsorbed on silica gel and subjected to FC (silica gel, column 15 × 3 cm, eluted with CH_2Cl_2/MeOH 95:5 → 90:10) affording one main zone. Evaporation of the solvent gave **3** (0.575 g, 62%) as a colorless solid. TLC (silica gel, CH_2Cl_2/MeOH 9:1). R_f 0.4. UV λ_{max} (MeOH)/nm 258 (ε/dm^3 mol^{-1} cm^{-1} 9900), 286 (10 900). ^{1}H NMR [DMSO-d_6, 300 MHz]: δ 2.21−2.29 (m, 1H, C2′-H$_\alpha$), 2.73−2.82 (m, 1H, C2′-H$_\beta$), 3.32−3.40 (m, 1H, C5′-H), 3.47−3.53 (m, 1H, C5′-H), 3.55 (t, J = 2.4 Hz, 1H, C≡CH), 3.79−3.84 (m, 1H, C4′-H), 4.29 (d, J = 2.4 Hz, 2H, CH_2), 4.39−4.45 (m, 1H, C3′-H), 4.55 (s, 2H, CH_2), 4.78 (t, J = 5.7 Hz, 1H, C5′-OH), 5.29 (d, J = 4.5 Hz, 1H, C3′-OH), 6.55 (t, J = 6.3 Hz, C1′-H), 8.24 (s, 1H, C2-H). Anal. Calcd for $C_{16}H_{17}N_5O_4$ (343.1281): C 55.97, H 4.99, N 20.40; Found: C 55.87, H 4.83, N 20.31.

1-[2-Deoxy-β-D-*erythro*-pentofuranosyl]-[3-(prop-2-ynyloxy)prop-1-ynyl]-4-{[(*N,N*-dimethylamino)-methylidene)]amino}-1*H*-pyrazolo[3,4-*d*]pyrimidine (10). To a solution of **3** (0.50 g, 1.45 mmol) in MeOH (50 mL) was added *N,N*-dimethylformamide dimethylacetal (4.34 g, 4.84 mL, 36.44 mmol) and the reaction mixture was stirred at rt for 30 min. Then the solvent was evaporated and the residue was subjected to FC (silica gel, column 10 × 4 cm, eluted with CH_2Cl_2/MeOH 97:3 → 90:10). Evaporation of the main zone afforded compound **10** (0.50 g, 86%) as a colorless foam. TLC (CH_2Cl_2/MeOH 9:1). R_f 0.5. UV λ_{max} (MeOH)/nm 324 (ε/dm^3 mol^{-1} cm^{-1} 20 300). ^{1}H NMR [DMSO-d_6, 300 MHz]: δ 2.24−2.32 (m, 1H, C2′-H$_\alpha$), 2.76−2.85 (m, 1H, C2′-H$_\beta$), 3.19 (s, 3H, CH_3), 3.23 (s, 3H, CH_3), 3.33−3.34 (m, 1H, C5′-H), 3.48−3.54 (m, 2H, C≡CH, C5′-H), 3.80−3.85 (m, 1H, C4′-H), 4.29 (d, J = 2.4 Hz, 2H, CH_2), 4.42−4.45 (m, 1H, C3′-H), 4.53 (s, 2H, CH_2), 4.79 (t, J = 5.7 Hz, 1H, C5′-OH), 5.31 (d, J = 4.5 Hz, 1H, C3′-OH), 6.60 (t, J = 6.3 Hz, 1H, C1′-H), 8.45 (s, 1H, C2-H),

dx.doi.org/10.1021/bc5003532 | *Bioconjugate Chem.* 2014, 25, 1855−1870

8.93 (s, 1H, NCH). ESI-TOF m/z calcd. for $C_{19}H_{22}N_6O_4$ [M + H^+] 399.1775, found 399.1797.

1-[2-Deoxy-5-*O*-(4,4′-dimethoxytrityl)-*β*-D-*erythro*-pentofuranosyl]-4-{[(*N*,*N*-dimethylamino)methylidene]-amino}-[3-(prop-2-ynyloxy)prop-1-ynyl]-1*H*-pyrazolo-[3,4-*d*]pyrimidine (11). Compound **10** (0.45 g, 1.13 mmol) was dried by repeated coevaporation with dry pyridine (3 × 5 mL). The residue was dissolved in dry pyridine (12 mL) and stirred with 4,4′-dimethoxytrityl chloride (0.46 g, 1.35 mmol) at rt for 4 h. After completion of the reaction (monitored by TLC), methanol (6 mL) was added to the reaction mixture and stirring was continued for another half an hour. The reaction mixture was evaporated to dryness under reduced pressure and the remaining residue was dissolved in dichloromethane (50 mL) and washed with 5% aq. $NaHCO_3$ solution (2 × 250 mL) and water (100 mL). The organic layer was dried over Na_2SO_4, and the solvent was evaporated under reduced pressure and the residue was subjected to FC (silica gel, column 10 × 4 cm, eluted with CH_2Cl_2/acetone 95:5 → 80:20). Evaporation of the main zone afforded **11** (0.42 g, 53%) as a colorless foam. TLC (silica gel, CH_2Cl_2/acetone 75:25). R_f 0.6. UV λ_{max} (MeOH)/nm 323 (ε/dm^3 mol^{-1} cm^{-1} 27 900). ^{1}H NMR [DMSO-d_6, 300 MHz]: δ 2.29−2.38 (m, 1H, C2′-H$_\alpha$), 2.79−2.87 (m, 1H, C2′-H$_\beta$), 2.97−3.09 (m, 2H, C5′-H), 3.19 (s, 3H, CH_3), 3.23 (s, 3H, CH_3), 3.55 (t, J = 2.4 Hz, 1H, C≡CH), 3.69 (s, 3H, OCH_3), 3.70 (s, 3H, OCH_3), 3.90−3.95 (m, 1H, C4′-H), 4.27 (d, J = 2.4 Hz, 2H, CH_2), 4.52−4.60 (m, 3H, CH_2, C3′-H), 5.34 (d, J = 4.8 Hz, 1H, C3′-OH), 6.61−6.64 (m, 1H, C1′-H), 6.70−6.77 (m, 4H, Ar-H), 7.13−7.21 (m, 7H, Ar-H), 7.28−7.31 (m, 2H, Ar-H), 8.49 (s, 1H, C2-H), 8.93 (s, 1H, NCH). ESI-TOF m/z calcd. for $C_{40}H_{40}N_6O_6$ [M + H^+] 701.3082, found 701.3070.

1-[2-Deoxy-5-*O*-(4,4′-dimethoxytrityl)-*β*-D-*erythro*-pentofuranosyl]-4-{[(*N*,*N*-dimethylamino)methylidene]-amino}-[3-(prop-2-ynyloxy)prop-1-ynyl]-1*H*-pyrazolo[3,4-*d*]pyrimidin-3′-(2-cyanoethyl)-*N*,*N*-diisopropylphosphoramidite (12). A solution of **11** (0.187 g, 0.266 mmol) in dry CH_2Cl_2 (15 mL) was stirred with (i-Pr)$_2$NEt (0.069 g, 89 μL, 0.53 mmol) at rt. Then, 2-cyanoethyl diisopropylphosphoramidochloridite (0.126 g, 118 μL, 0.53 mmol) was added and the reaction mixture was stirred for 30 min. After completion of the reaction (monitored by TLC), the reaction mixture was diluted with CH_2Cl_2 (40 mL) and was poured into 5% $NaHCO_3$ solution (40 mL) and extracted with CH_2Cl_2 (3 × 40 mL). The combined organic phases were dried over Na_2SO_4 and the solvent was evaporated. The residual foam was applied to FC (silica gel, column 8 × 3 cm, eluted with CH_2Cl_2/acetone 100:0 → 95:5). Evaporation of the main zone afforded **12** (0.15 g, 62%) as a colorless foam. TLC (silica gel, CH_2Cl_2/acetone 8:2). R_f 0.6. ^{31}P NMR ($CDCl_3$, 121 MHz): 148.46, 148.37. ESI-TOF m/z calcd. for $C_{49}H_{57}N_8O_7P$ [M + H^+] 901.4161, found 901.4136.

4-Amino-1-[2-deoxy-*β*-D-*erythro*-pentofuranosyl]-3-[(methylanthracene-1′,2′,3′-triazol-4′-yl)-1*H*-pyrazolo-[3,4-*d*]pyrimidine (13). To a solution of **2** (0.10 g, 0.36 mmol) and anthracene azide **5** (0.10 g, 0.43 mmol) in THF:H_2O:t-BuOH,(3:1:1, 5 mL) was added sodium ascorbate (361 μL, 0.36 mmol) of a freshly prepared 1 M solution in water, followed by the addition of copper(II) sulfate pentahydrate 7.5% in water (311 μL, 0.36 mmol). The reaction mixture was stirred for 12 h at rt and the solution was evaporated, and applied to FC (silica gel, column 10 × 3 cm, CH_2Cl_2/MeOH 88:12). From the main zone compound **13** (0.137 g, 74%) was isolated as a yellowish foam. TLC (silica gel, CH_2Cl_2/MeOH 8:2). R_f 0.4. λ_{max}(MeOH)/nm 260 (ε/dm^3 mol^{-1} cm^{-1} 33 200), 355 (93 00), 376 (84 00). ^{1}H NMR [DMSO-d_6, 300 MHz]: δ 2.20−2.27 (m, 1H, C2′-H$_\alpha$), 2.77−2.86 (m, 1H, C2′-H$_\beta$), 3.51−3.53 (m, 1H, C5′-H), 3.82−3.83 (m, 1H, C4′-H), 4.44 (s, 1H, C3′-H), 4.82 (s, 1H, C5′-OH), 5.28 (s, 1H, C3′-OH), 6.53−6.57 (t, J 6.3 Hz, 1H, C1′-H), 6.78 (s, 2H, Ar-H), 7.56−7.70 (m, 4H, Ar-H), 8.05 (s, 1H, triazole−H), 8.16−8.19 (d, J = 9.0 Hz, 2H, Ar-H, C2-H), 8.66−8.69 (d, J = 9.0 Hz, 2H, Ar-H), 8.74−8.76 (d, J = 6.6 Hz, 2H, Ar-H), 9.0 (s, 1H, Ar-H). Anal. Calcd for $C_{27}H_{24}N_8O_3$: C 63.77, H 4.76, N 22.03. Found: C 63.86, H 4.90, N 21.91.

2-Deoxy-*β*-D-*erythro*-pentofuranosyl-[3-(9,10-bis-(methyleneanthracene-1*H*-1,2,3-triazole-1,4-diyl-hexyne-6,1-diyl)]-1*H*-pyrazolo[3,4-*d*]-pyrimidin-4-amine (15). To a solution of compound **1**[26] (0.148 g, 0.41 mmol) and **4** (0.060 g, 0.20 mmol) in THF:H_2O:t-BuOH, 3:1:1, (5 mL), was added a freshly prepared 1 M solution of sodium ascorbate (345 μL, 0.34 mmol) in water, followed by the addition of copper(II) sulfate pentahydrate 7.5% in water (278 μL, 0.08 mmol) and the reaction mixture was stirred at room temperature for 12 h. After completion of the reaction (monitored by TLC), the reaction mixture was evaporated, and applied to flash chromatography (FC) (silica gel, column 10 × 3 cm, CH_2Cl_2−MeOH, 85:15). From the main zone compound **15** (0.147 g, 70%) was isolated as a pale yellow solid. TLC (silica gel, CH_2Cl_2−MeOH, 90:10): R_f 0.4. λ_{max} (MeOH)/nm 258 (ε/dm^3 mol^{-1} cm^{-1} 149 600), 260 (107 000), 354 (7400), 361 (12 400), 394 (12 900). ^{1}H NMR (DMSO-d_6, 300 MHz): δ 1.56−1.64 (m, 8H, 4 × CH_2), 2.19−2.27 (m, 2H, 2 × C2′-H$_\alpha$), 2.49−2.57 (m, 8H, 4 × CH_2), 2.72−2.80 (m, 2H, 2 × C2′-H$_\beta$), 3.48−3.54 (m, 2H, 2 × C5′-H), 3.78−3.83 (m, 2H, 2 × C4′-H), 4.41 (br s, 2H, 2 × C3′-H), 4.81 (br s, 2H, C5′-OH), 5.30 (br s, 2H, 2 × C3′-OH), 6.52 (t, J = 6.3 Hz, 2H, 2 × C1′-H), 6.62 (s, 4H, 2 × CH_2), 7.64−7.68 (m, 4H, 2 × triazole-H, 2 × Ar-H), 7.75 (s, 4H, Ar-H), 8.22 (s, 2H, 2 × C2-H), 8.65−8.68 (m, 4H, Ar-H). Anal. calcd for $C_{52}H_{54}N_{16}O_6$ (999.1): C 62.51, H 5.45, N, 22.43. Found: C 62.60, H 5.50, N 22.31.

2-Deoxy-*β*-D-*erythro*-pentofuranosyl-[3-(9,10-bis-(methyleneanthracene-1*H*-1,2,3-triazole)]-1*H*-pyrazolo-[3,4-*d*]-pyrimidin-4-amine (16). Procedure as described above for compound **15**. Compound **2**[36] (0.100 g, 0.36 mmol) and **4** (0.052 g, 0.18 mmol), THF:H_2O:t-BuOH, 3:1:1, (3 mL), 1 M solution of sodium ascorbate (293 μL, 0.29 mmol), copper(II) sulfate pentahydrate 7.5% in water (240 μL, 0.07 mmol). (FC) (silica gel, column 10 × 3 cm, CH_2Cl_2−MeOH, 90:10). From the main zone compound **16** (0.051 g, 33%) was isolated as a pale yellow solid. TLC (silica gel, CH_2Cl_2−MeOH, 85:15): R_f 0.35. λ_{max} (MeOH)/nm 257 (ε/dm^3 mol^{-1} cm^{-1} 149 000), 260 (101 400), 354 (7500), 373 (12 000), 394 (12 700). ^{1}H NMR (DMSO-d_6, 300 MHz): δ 2.20−2.28 (m, 2H, 2 × C2′-H$_\alpha$), 2.78−2.87 (m, 2H, 2 × C2′-H$_\beta$), 3.38−3.44 (m, 2H, 2 × C5′-H), 3.51−3.56 (m, 2H, 2 × C5′-H), 3.80−3.83 (m, 2H, 2 × C4′-H), 4.44−4.47 (m, 2H, 2 × C3′-H), 4.82 (t, J = 6.0 Hz, 2H, 2 × C5′-OH), 5.28 (d, J = 4.5 Hz, 2H, 2 × C3′-OH), 6.56 (t, J = 6.3 Hz, 2H, 2 × C1′-H), 6.85 (s, 4H, 2 × CH_2), 7.72−7.76 (m, 4H, Ar-H), 8.01 (br s, 2H, NH_2), 8.19 (s, 2H, 2 × triazole-H), 8.76−8.80 (m, 4H, Ar-H), 8.85 (s, 2H, 2 × C2-H), 8.97 (br s, 2H NH_2). ESI-TOF m/z calcd. for $C_{40}H_{38}N_{16}O_6$ [M + Na^+] 861.3052, found 861.3020.

2-Deoxy-*β*-D-*erythro*-pentofuranosyl-[3-(9,10-bis-(methyleneanthracene-1*H*-1,2,3-triazole-3-(prop-2-yn-1-yloxy)prop-1-yne)]-1*H*-pyrazolo[3,4-*d*]-pyrimidin-4-amine (17). Procedure as described above for compound **15**. Compound **3** (0.100 g, 0.29 mmol) and **4** (0.042 g, 0.15 mmol), THF:H_2O:t-BuOH, 3:1:1, (3 mL), 1 M solution of sodium

dx.doi.org/10.1021/bc5003532 | Bioconjugate Chem. 2014, 25, 1855−1870

ascorbate (240 μL, 0.24 mmol), copper(II) sulfate pentahydrate 7.5% in water (195 μL, 0.06 mmol). (FC) (silica gel, column 10 × 3 cm, CH_2Cl_2−MeOH, 90:10). From the main zone compound **17** (0.068 g, 48%) was isolated as a pale yellow solid. TLC (silica gel, CH_2Cl_2−MeOH, 80:20): R_f 0.9. λ_{max} (MeOH)/nm 258 (ε/dm^3 mol^{-1} cm^{-1} 119 000), 260 (92 000), 354 (6300), 373 (10 200), 394 (10 500). ^{1}H NMR (DMSO-d_6, 300 MHz): δ 2.20−2.28 (m, 2H, 2 × C2′-H$_\alpha$), 2.72−2.80 (m, 2H, CH_2), 3.02−3.11 (m, 2H, 2 × C2′-H$_\beta$), 3.35−3.53 (m, 4H, 2 × C5′-H), 3.78−3.83 (m, 2H, 2 × C4′-H), 4.44 (s, 6H, 2 × C3′-H, 2 × CH_2), 4.55 (s, 4H, 2 ×CH_2), 4.78 (br s, 2H, C5′-OH), 5.28 (br s, 2H, 2 × C3′-OH), 6.54 (t, J = 6.3 Hz, 2H, 2 × C1′-H), 6.69 (s, 4H, 2 × CH_2), 7.67−7.70 (m, 4H, Ar-H), 8.06 (s, 2H, 2 × triazole-H), 8.24 (s, 2H, 2 × C2-H), 8.66−8.70 (m, 4H, Ar-H). ESI-TOF calcd for $C_{48}H_{46}N_{16}O_8$ [M + Na]$^+$: 997.3577; m/z found: 997.3576.

General Procedure for High-Density Functionalization of Oligonucleotides. To the single stranded oligonucleotide **24** (3.0 A_{260} units, 50 μmol) were added a mixture of a $CuSO_4$-TBTA ligand complex (30 μL of 20 mmol solution of $CuSO_4$ in H_2O/*t*-BuOH/DMSO (1:1:3) and 30 μL of 20 mmol solution of TBTA in *t*-BuOH/DMSO (1:3), tris(carboxyethyl)-phosphine (TCEP; 30 μL of 20 mmol solution in H_2O), sodium bicarbonate ($NaHCO_3$, 30 μL of 100 mmol solution in H_2O), azide **5** (50 μL of 20 mmol stock solution in THF), and 30 μL of DMSO, and then the reaction mixture was stirred at room temperature for 12 h. The reaction mixture was concentrated in a Speed Vac, dissolved in 0.2 mL of bidistilled water, and centrifuged for 20 min at 14 000 rpm. The supernatant was collected and further purified by reversed phase HPLC, using gradient I to give about 50% (1.5 A_{260} units) of the cross-linked oligonucleotide **29**. The other high-density labeled oligonucleotides were prepared in a similar way.

General Procedure for the Cross-Linking of Oligonucleotides. To the single stranded oligonucleotide **20** (3.0 A_{260} units, 50 μmol) were added a mixture of a $CuSO_4$-TBTA ligand complex (30 μL of 20 mmol solution of $CuSO_4$ in H_2O/*t*-BuOH/DMSO (1:1:3) and 30 μL of 20 mmol solution of TBTA in *t*-BuOH/DMSO (1:3), tris(carboxyethyl)-phosphine (TCEP; 30 μL of 20 mmol solution in H_2O), sodium bicarbonate (30 μL of 100 mmol solution in H_2O), the bis-azide **4** (2.5 μL of 20 mmol stock solution in THF), and 30 μL of DMSO, and then the reaction mixture was stirred at room temperature for 12 h. The reaction mixture was concentrated in a Speed Vac, dissolved in 0.2 mL of bidistilled water, and centrifuged for 20 min at 14 000 rpm. The supernatant was collected and further purified by reversed phase HPLC, using gradient II to give about 50% (1.5 A_{260} units) of the cross-linked oligonucleotide **42**. The other cross-linked oligonucleotides were prepared in a similar way.

Ion-Exchange Chromatography. Ion-exchange chromatography was performed on a 4 × 250 mm DNA PA-100 column with a precolumn using a HPLC apparatus. Elution profiles were recorded at 260 nm. The alkynylated or cross-linked oligonucleotides (0.1 A_{260} units each) were dissolved in 100 μL of water and then directly injected into the apparatus. The compounds were eluted using the following gradient: (A) 25 mM Tris-HCl, 10% MeCN, pH 7.0; (B) 25 mM Tris-HCl, 1.0 M NaCl, and 10% MeCN, pH 7.0. Elution gradient: 0−30 min 20−80% B in A with a flow rate of 0.75 mL min^{-1}.

■ ASSOCIATED CONTENT

Supporting Information

MALDI-TOF mass table, ^{1}H−^{13}C coupling constants, HPLC profiles and ^{1}H, ^{13}C, DEPT-135, and ^{1}H−^{13}C gated-decoupled NMR spectra. This material is available free of charge via the Internet at http://pubs.acs.org.

■ AUTHOR INFORMATION

Corresponding Author

*Phone: +49(0)251 53406 500. Fax: +49(0)251 53406 857. E-mail: Frank.Seela@uni-osnabrueck.de. Web: www.seela.net.

Notes

The authors declare no competing financial interest.

■ ACKNOWLEDGMENTS

We thank Dr. Peter Leonard and Dr. S. Budow-Busse for helpful discussions and support while preparing the manuscript. We also thank Mr. H. Mei for measuring the NMR spectra and Mr. Nhat Quang Tran for the oligonucleotide syntheses. We thank Dr. M. Letzel, Organisch-Chemisches Institut, Universität Münster, Münster, Germany, for the measurement of the MALDI spectra. Financial support by ChemBiotech, Münster, Germany, is highly appreciated.

■ REFERENCES

(1) McLaughlin, C. K., Hamblin, G. D., and Sleiman, H. F. (2011) Supramolecular DNA assembly. *Chem. Soc. Rev. 40*, 5647−5656.

(2) He, Y., Ye, T., Su, M., Zhang, C., Ribbe, A. E., Jiang, W., and Mao, C. (2008) Hierarchical self-assembly of DNA into symmetric supramolecular polyhedra. *Nature 452*, 198−202.

(3) Bracha, D., and Bar-Ziv, R. H. (2014) Dendritic and nanowire assemblies of condensed DNA polymer brushes. *J. Am. Chem. Soc. 136*, 4945−4953.

(4) Nesterova, I. V., and Nesterov, E. E. (2014) Rational design of highly responsive pH sensors based on DNA i-motif. *J. Am. Chem. Soc. 136*, 8843−8846.

(5) Endo, M., and Majima, T. (2003) Parallel, double-helix DNA nanostructures using interstrand cross-linked oligonucleotides with bismaleimide linkers. *Angew. Chem., Int. Ed. 42*, 5744−5747.

(6) Li, T., and Famulok, M. (2013) I-Motif-programmed functionalization of DNA nanocircles. *J. Am. Chem. Soc. 135*, 1593−1599.

(7) Barrangou, R. (2012) RNA-mediated programmable DNA cleavage. *Nat. Biotechnol. 30*, 836−838.

(8) Endo, M., Seeman, N. C., and Majima, T. (2005) DNA tube structures controlled by a four-way-branched DNA connector. *Angew. Chem., Int. Ed. 44*, 6074−6077.

(9) Idili, A., Vallée-Bélisle, A., and Ricci, F. (2014) Programmable pH-triggered DNA nanoswitches. *J. Am. Chem. Soc. 136*, 5836−5839.

(10) Matray, T. J., and Kool, E. T. (1998) Selective and stable DNA base pairing without hydrogen bonds. *J. Am. Chem. Soc. 120*, 6191−6192.

(11) Randolph, J. B., and Waggoner, A. S. (1997) Stability, specificity and fluorescence brightness of multiply-labeled fluorescent DNA probes. *Nucleic Acids Res. 25*, 2923−2929.

(12) Kiviniemi, A., Virta, P., and Lönnberg, H. (2008) Utilization of intrachain 4′-C-azidomethylthymidine for preparation of oligodeoxyribonucleotide conjugates by click chemistry in solution and on a solid support. *Bioconjugate Chem. 19*, 1726−1734.

(13) Gierlich, J., Burley, G. A., Gramlich, P. M. E., Hammond, D. M., and Carell, T. (2006) Click chemistry as a reliable method for the high-density postsynthetic functionalization of alkyne-modified DNA. *Org. Lett. 8*, 3639−3642.

(14) Zhang, G., Surwade, S. P., Zhou, F., and Lir, H. (2013) DNA nanostructure meets nanofabrication. *Chem. Soc. Rev. 42*, 2488−2496.

(15) Zheng, H., Xiao, M., Yan, Q., Ma, Y., and Xiao, S.-J. (2014) Small circular DNA molecules act as rigid motifs to build DNA nanotubes. *J. Am. Chem. Soc. 136*, 10194−10197.
(16) Suzuki, Y., Endo, M., Yang, Y., and Sugiyama, H. (2014) Dynamic assembly/disassembly processes of photoresponsive DNA origami nanostructures directly visualized on a lipid membrane surface. *J. Am. Chem. Soc. 136*, 1714−1717.
(17) Alexander, C. M., Hamner, K. L., Maye, M. M., and Dabrowiak, J. C. (2014) Multifunctional DNA-gold nanoparticles for targeted doxorubicin delivery. *Bioconjugate Chem. 25*, 1261−1271.
(18) Cimino, G. D., Shi, Y.-B., and Hearst, J. E. (1986) Wavelength dependence for the photoreversal of a psoralen-DNA cross-link. *Biochemistry 25*, 3013−3020.
(19) Summerfield, F. W., and Tappel, Al. L. (1983) Determination by fluorescence quenching of the environment of DNA crosslinks made by malondialdehyde. *Biochim. Biophys. Acta 740*, 185−189.
(20) Haque, M. M., Sun, H., Liu, S., Wang, Y., and Peng, X. (2014) Photoswitchable formation of a DNA interstrand cross-link by a coumarin-modified nucleotide. *Angew. Chem., Int. Ed. 53*, 7001−7005.
(21) Noronha, A. M., Noll, D. M., Wilds, C. J., and Miller, P. S. (2002) N^4C−Ethyl−N^4C cross-linked DNA:Synthesis and characterization of duplexes with interstrand cross-links of different orientations. *Biochemistry 41*, 760−771.
(22) Huisgen, R., Szeimies, G., and Möbius, L. (1967) 1.3-Dipolare Cycloadditionen, XXXII. Kinetik der additionen organischer azide an CC-mehrfachbindungen. *Chem. Ber. 100*, 2494−2507.
(23) Tornøe, C. W., Christensen, C., and Meldal, M. (2002) Peptidotriazoles on solid phase: [1,2,3]-Triazoles by regiospecific copper(I)-catalyzed 1,3-dipolar cycloadditions of terminal alkynes to azides. *J. Org. Chem. 67*, 3057−3064.
(24) Rostovtsev, V. V., Green, L. G., Fokin, V. V., and Sharpless, K. B. (2002) A stepwise Huisgen cycloaddition process: Copper(I)-catalyzed regioselective "ligation" of azides and terminal alkynes. *Angew. Chem., Int. Ed. 41*, 2596−2599.
(25) Meldal, M., and Tornøe, C. W. (2008) Cu-catalyzed azide-alkyne cycloaddition. *Chem. Rev. 108*, 2952−3015.
(26) Seela, F., and Pujari, S. S. (2010) Azide-alkyne "click" conjugation of 8-aza-7-deazaadenine-DNA: Synthesis, duplex stability and fluorogenic dye labelling. *Bioconjugate Chem. 21*, 1629−1641.
(27) Pujari, S. S., Xiong, H., and Seela, F. (2010) Cross-linked DNA generated by "bis-click" reactions with bis-functional azides: Site independent ligation of oligonucleotides *via* nucleobase alkynyl chains. *J. Org. Chem. 75*, 8693−8696.
(28) Ingale, S. A., and Seela, F. (2013) Stepwise click functionalization of DNA through a bifunctional azide with a chelating and a nonchelating azido group. *J. Org. Chem. 78*, 3394−3399.
(29) Pujari, S. S., and Seela, F. (2012) Cross-linked DNA: Propargylated ribonucleosides as "click" ligation sites for bifunctional azides. *J. Org. Chem. 77*, 4460−4465.
(30) Pujari, S. S., Leonard, P., and Seela, F. (2014) Oligonucleotides with "clickable" sugar residues: Synthesis, duplex stability and terminal versus central interstrand cross-linking of 2′-*O*-propargylated 2-aminoadenosine with a bifunctional azide. *J. Org. Chem. 79*, 4423−4437.
(31) Pujari, S. S., and Seela, F. (2013) Parallel stranded DNA stabilized with internal sugar cross-links: Synthesis and click ligation of oligonucleotides containing 2′-propargylated isoguanosine. *J. Org. Chem. 78*, 8545−8561.
(32) Grundberg, H. E., Wendt, O. F., and Nilsson, U. J. (2004) Synthesis and conformational analysis of 9,10-bis-aminomethyl-11,12-dicarboxy-dibenzobarrelene derivatives. *Tetrahedron Lett. 45*, 6083−6085.
(33) Huang, H.-J., Fang, H.-Y., Chir, J.-L., and Wu, A. T. (2011) Effect of bis-triazoles on a ribose-based fluorescent sensor. *Luminescence 26*, 518−522.
(34) Xie, F., Sivakumar, K., Zeng, Q., Bruckman, M. A., Hodges, B., and Wang, Q. (2008) *Tetrahedron 64*, 2906−2914.
(35) Malakhov, A. D., Skorobogatyi, M. V., Prokhorenko, I. A., Gontarev, S. V., Kozhich, D. T., Stetsenko, D. A., Stepanova, I. A., Shenkarev, Z. O., Berlin, U. A., and Korshun, V. A. (2004) 1-(Phenylethynyl)pyrene and 9,10-bis(phenylethynyl)anthracene, useful fluorescent dyes for DNA labeling: Excimer formation and energy transfer. *Eur. J. Org. Chem.*, 1298−1307.
(36) Seela, F., Pujari, S. S., and Schäfer, A. H. (2011) Hydrogelation and spontaneous fiber formation of 8-aza-7-deazaadenine nucleoside "click" conjugates. *Tetrahedron 67*, 7418−7425.
(37) Seela, F., He, Y., He, J., Becher, G., Kröschel, R., Zulauf, M., and Leonard, P. (2004) Base-modified oligonucleotides with increased duplex stability. Pyrazolo[3,4-d] pyrimidines replacing purines. In *Oligonucleotide Synthesis: Methods and Applications (Methods in Molecular Biology)* (Herdenwijn, P., Ed.) pp 165−186, Humana Press Inc..
(38) Seela, F., Zulauf, M., Sauer, M., and Deimel, M. (2000) 7-Substituted 7-deaza-2′-deoxyadenosines and 8-aza-7-deaza-2′-deoxyadenosines: Fluorescence of DNA base analogues induced by the 7-alkynyl side chain. *Helv. Chim. Acta 83*, 910−927.
(39) Seela, F., and Zulauf, M. (1999) Oligonucleotides containing 7-deazaadenines: The influence of the 7-substituent chain length and charge on the duplex stability. *Helv. Chim. Acta 82*, 1878−1898.
(40) Seela, F., and Zulauf, M. (1999) Synthesis of oligonucleotides containing pyrazolo[3,4-*d*]pyrimidines: The influence of 7-substituted 8-aza-7-deazaadenines on the duplex structure and stability. *J. Chem. Soc., Perkin Trans. 1*, 479−488.
(41) Ichikawa, S., Ueno, H., Sunadome, T., Sato, K., and Matsuda, A. (2013) Tris(azidoethyl)amine hydrochloride; a versatile reagent for synthesis of functionalized dumbbell oligodeoxynucleotides. *Org. Lett. 15*, 694−697.
(42) Abe, N., Abe, H., and Ito, Y. (2007) Dumbbell-shaped nanocircular RNAs for RNA interference. *J. Am. Chem. Soc. 129*, 15108−15109.
(43) Higuchi, Y., Furukawa, K., Miyazawa, T., and Minakawa, N. (2014) Development of a new dumbbell-shaped decoy DNA using a combination of the unnatural base pair ImO^N:NaN^O and a CuAAC reaction. *Bioconjugate Chem. 25*, 1360−1369.
(44) van Dongen, S. F. M., Clerx, J., Nørgaard, K., Bloemberg, T. G., Cornelissen, J. J. L. M., Trakselis, M. A., Nelson, S. W., Benkovic, S. J., Rowan, A. E., and Nolte, R. J. M. (2013) A clamp-like biohybrid catalyst for DNA oxidation. *Nat. Chem. 5*, 945−951.
(45) Duff, M. R., Mudhivarthi, V. K., and Kumar, C. V. (2009) Rational design of anthracene-based DNA binders. *J. Phys. Chem. B 113*, 1710−1721.
(46) Chang, K. C., Su, I., Senthilvelan, A., and Chung, W. (2007) Triazole-modified calix[4]crown as a novel fluorescent on-off switchable chemosensor. *Org. Lett. 9*, 3363−3366.
(47) Ghosh, K., Masanta, G., and Chattopadhyay, A. P. (2009) Anthracene labeled pyridine amides: A class of prototype PET sensors towards monocarboxylic acid. *J. Photochem. Photobiol. 203*, 40−49.
(48) Li, X., Zang, G., Ma, H., Zang, D., Li, J., and Zhu, D. (2004) 4,5-Dimethylthio-4¢-[2-(9-anthryloxy)ethylthio]tetrathiafulvalene, a highly selective and sensitive chemiluminescence probe for singlet oxygen. *J. Am. Chem. Soc. 126*, 11543−11548.
(49) Burnelle, L., Lahiri, J., and Detrano, R. (1968) On the photodimerization of anthracene and its mesosubstituted derivatives. *Tetrahedron 24*, 3517−3531.
(50) Ihara, T., Fujii, T., Mukae, M., Kitamura, Y., and Jyo, A. (2004) Photochemical ligation of DNA conjugates through anthracene cyclodimer formation and its fidelity to the template sequences. *J. Am. Chem. Soc. 126*, 8880−8881.
(51) Ogawa, M., Shirai, H., Kuroda, K., and Kato, C. (1992) Solid-state intercalation of naphthalene and anthracene into alkylammonium-montmorillonites. *Clays Clay Minerals 40*, 485−490.
(52) Lebreton, P. R. (1985) The intercalation of benzo[a]pyrene and 7,12-dimethylbenz[a]anthracene metabolites and metabolite model compounds into DNA. *ACS Symp. Ser. 283*, 209−238.
(53) Moran, N., Bassani, D. M., Desvergne, J.-P., Keiper, S., Lowden, P. A. S., Vyle, J. S., and Tucker, J. H. R. (2006) Detection of a single DNA base-pair mismatch using an anthracenetagged fluorescent probe. *Chem. Commun.*, 5003−5005.

(54) Saito, Y., Motegi, K., Sekhar Bag, S., and Saito, I. (2008) Anthracene based base-discriminating fluorescent oligonucleotide probes for SNPs typing: Synthesis and photophysical properties. *Bioorg. Med. Chem. 16*, 107−113.